TReSpire — a biophysical TRee Stem respiration model

Roberto L. Salomon[1], Linus De Roo[1], Jacek Oleksyn[2], Dirk J. W. De Pauw[1], Kathy Steppe[1]

[1] Laboratory of Plant Ecology, Faculty of Bioscience Engineering, Ghent University, Coupure links 653, 9000 Ghent, Belgium

[2] Polish Academy of Sciences, Institute of Dendrology, Parkowa 5, PL-62-035 Kórnik, Poland

Corresponding author: RobertoLuis.SalomonMoreno@UGent.be; +32 9 264 61 14

ORCIDs:

Roberto L. Salomon: 0000-0003-2674-1731

Linus de Roo: 0000-0002-3627-1406

Jacek Oleksyn: 0000-0002-6576-3258

Kathy Steppe: 0000-0001-6252-0704

Total word counting: 7576

Introduction: 1209

Materials and methods: 3431

Results: 742

Discussion: 2104

Figures: 5 (1, 2, 3 and 5 in colour)

Tables: 4

Abstract

Mechanistic models of plant respiration remain poorly developed, especially in stems and woody tissues where measurements of CO_2 efflux do not necessarily reflect local respiratory activity.

We built a process-based model of stem respiration that couples water and carbon fluxes at the organ level (TReSpire). To this end, sap flow, stem diameter variations, xylem and soil water potential, stem temperature, stem CO_2 efflux, and nonstructural carbohydrates were measured in a maple tree, while xylem CO_2 concentration and additional stem and xylem diameter variations were monitored in an ancillary tree for model validation.

TReSpire realistically described (i) turgor pressure to differentiate growing from non-growing metabolism, (ii) maintenance expenditures in xylem and outer tissues based on Arrhenius kinetics and nitrogen content, and (iii) radial CO_2 diffusivity and CO_2 solubility and transport in the sap solution. Collinearity issues with phloem unloading rates and sugar-starch interconversion suggest parallel sub-modelling to close the stem carbon balance.

TReSpire brings a breakthrough in the modelling of stem water and carbon fluxes at a detailed (hourly) temporal resolution. TReSpire is calibrated from a sink-driven perspective, and has potential to advance our understanding on stem growth dynamics, CO_2 fluxes and underlying respiratory physiology across different species and phenological stages.

Keywords

CO_2 efflux, growth and maintenance respiration, plant modelling, sink demand, stem carbon balance, stem respiration, turgor-driven growth, xylem CO_2 transport

Introduction

As trees grow, biomass is mostly allocated to stems and branches, which constitute the largest living sink of anthropogenic CO_2 emissions at the global scale (Cuny *et al.*, 2015). To fulfil stem metabolic activities, assimilated carbon (C) is partially consumed via respiratory processes, and CO_2 is emitted back to the atmosphere as a by-product. Thus, despite uncertainty in estimates of stem respiration (R_S) at large spatial scales, R_S is expected to play a major role in ecosystem C balances, with stem CO_2 efflux to the atmosphere (E_A) accounting for 5-35% of ecosystem respiration (Campioli *et al.*, 2016; Salomón *et al.*, 2017), and being 11% and 20% of the amount of ecosystem gross and net primary production (GPP and NPP, respectively) (Yang *et al.*, 2016). Nevertheless, our understanding of stem and woody tissue respiration is deficient, especially when compared with our knowledge of CO_2 exchange at the leaf level (Meir *et al.*, 2017; Fatichi *et al.*, 2019). This is clearly illustrated by how woody tissue respiration is estimated by leading terrestrial biosphere models (TBMs). Most TBMs partition whole-plant (and hence woody tissue) respiration into two components according to the *growth-and-maintenance-respiration paradigm* (GMRP) postulated in the early 1970s (reviewed by Atkin et al., 2017): (i) Maintenance respiration (R_M) is commonly extrapolated from estimates of leaf dark respiration to stem and roots according to N allocation patterns across tree organs and assuming the same N-R_M relationship for leaves, stem and roots, despite evidence challenging this approach (Reich *et al.*, 2008). (ii) Growth respiration (R_G) is assumed to be a fixed fraction of NPP or GPP minus R_M. The latter assumption simplifies quantification of the respiratory costs associated with synthesis of new tissues, whose parametrization is responsible for the largest source of uncertainty of NPP in TBMs (ca. 50% in hardwood plant functional types and 30% in evergreen and non-woody ones; Dietze *et al.*, 2014). Overall, the fraction of autotrophic respiration that occurs in stems and roots (22% and 38%, respectively, according to an inter-biome comparison; see Campioli *et al.*, 2016) is ultimately derived from our better understanding of leaf respiratory metabolism, despite respiratory differences between photosynthetic and non-photosynthetic tissues (Armstrong *et al.*, 2006) and organs (Reich *et al.*, 2008).

Methodological feasibility has largely constrained our knowledge on stem (and woody tissue) respiration. While leaf photosynthesis and respiration can be directly estimated from measurements of CO_2 exchange in (apical) leaves enclosed in sealed chambers, CO_2 efflux from the stem does not necessarily reflect the respiratory activity of underlying tissues (Teskey *et al.*, 2008; Trumbore

et al., 2013). Respired CO_2 in the stem can radially diffuse to the atmosphere, axially diffuse along the stem in the gas phase (De Roo *et al.*, 2019), be fixed by anaplerotic reactions or woody tissue photosynthesis (Ávila *et al.*, 2014; Hilman *et al.*, 2018), or dissolve in the sap solution and be transported upward with the transpiration stream, which likely confound the interpretation of E_A measurements to the greatest extent (reviewed by Teskey *et al.*, 2008, 2017). To account for diverse fates of respired CO_2 in the stem, several methodological approaches have been proposed (McGuire & Teskey, 2004; Angert *et al.*, 2012; Salomón *et al.*, 2019a). However, there is not a universal and well-established protocol to bring them together and measure R_S in a way that could facilitate comparison among experiments. Not surprisingly, there is no consensus on the scalar (surface, volume or mass) in which R_S and E_A should be expressed (Meir *et al.*, 2017), nor on their terminology. In the context of climate change, a number of studies have shown downregulation of R_S in drought-stressed trees (see Rodríguez-Calcerrada *et al.*, 2014; and references therein), whereas contrasting results (see Rowland *et al.*, 2018; and references therein) evidence our deficient understanding of the effect of drought on woody tissue respiration. Likewise, elevated atmospheric CO_2 can result in a positive, neutral or negative effect on R_S (see Salomón *et al.*, 2019b; and references therein). So far, there are no theoretical frameworks that could reconcile disparity among these context-dependent observations and make consistent predictions of stem and woody tissue respiration under changing climate regimes.

From a biochemical perspective, CO_2 production encompasses a wide array of metabolic processes difficult to quantify (Sweetlove *et al.*, 2013; Tcherkez, 2017), and therefore "*plant respiratory regulation is too complex for a mechanistic representation in current terrestrial productivity models for carbon accounting and global change research*" (Gifford, 2003). We are not yet able to model whole-tree respiration at the same biochemical detail as we do for photosynthesis via the well-known Farquhar *et al.* (1980) model (Atkin *et al.*, 2014). Nevertheless, we do have the basis to build biophysical models of R_S at the organ level. Several models simulate stem hydraulic functioning (e.g. Steppe *et al.*, 2006, 2008; Chan *et al.*, 2016; Mencuccini *et al.*, 2017; Coussement *et al.*, 2018), phloem transport (e.g. Thompson & Holbrook, 2003; Minchin & Lacointe, 2017), and coupled water and C fluxes along the stem (e.g. Lacointe & Minchin, 2008; Hölttä *et al.*, 2009; De Schepper & Steppe, 2010). These approaches provide key information on the hydric and osmotic status of stem living cells that regulate their respiratory metabolism. Some of these models simulate cell turgor pressure, a critical driver of cell growth (Steppe *et al.*, 2006, 2008, 2015; Fatichi *et al.*,

2014; Coussement *et al.*, 2018), and further separate irreversible plastic stem growth from elastic fluctuations in bark water content (Steppe *et al.*, 2006; Mencuccini *et al.*, 2017). This is an essential step to disentangle growth from maintenance metabolism on a sub-daily basis (Saveyn *et al.*, 2007; Steppe *et al.*, 2015; Salomón *et al.*, 2018), and to consider plant respiration within sink-source theoretical frameworks (Atkin *et al.*, 2014; Fatichi *et al.*, 2019). By combining these process-based models with knowledge on thermal regulation (Ryan, 1991; Tjoelker *et al.*, 2001) and nitrogen (N) dependency (Ryan, 1991; Reich *et al.*, 2008) of respiratory processes within the GMRP (Amthor, 2000), it is feasible to model R_S at the organ level, and simulate diffusion and solubility of respired CO_2 within woody tissues according to CO_2 gradients along the xylem-atmosphere continuum and equilibrium reactions at the gaseous-liquid interface (McGuire & Teskey, 2002; Hölttä & Kolari, 2009). Furthermore, stem C sources (phloem unloading, starch depolymerization, woody tissue photosynthesis and anaplerotic fixation) fueling C sinks (respiration, growth, starch synthesis and osmoregulation) could be quantified to close the stem C balance (Lacointe & Minchin, 2008; De Schepper & Steppe, 2010) and eventually incorporate biophysical processes into whole-plant and large-scale models.

The main goal of this work is to develop a TRee Stem respiration model (TReSpire). To this end, R_S and associated respiratory fluxes were represented by process-based equations integrating (i) stem allometry, (ii) function and location of different woody tissues, (iii) stem water and C fluxes, (iv) cell turgor to differentiate growing from non-growing metabolism on a sub-daily basis, (v) temperature driven Arrhenius kinetics, (vi) N-dependency of respiratory processes, (vii) CO_2 diffusivity in the gas phase and its solubility in the sap solution, and (viii) C sources fuelling respiratory metabolism and additional stem C sinks. We pursue building a mechanistic model able to realistically describe R_S under varying biotic and abiotic conditions to advance knowledge in the respiratory physiology of woody tissues.

Materials and Methods

Description

Model overview. TReSpire describes geometrically the stem as two coaxial cylinders separated by the cambial layer: the xylem compartment and the outer tissues compartment, which integrates phloem and bark tissues (Génard *et al.*, 2001; Steppe *et al.*, 2006). Briefly, TReSpire is composed by three sub-models (Fig. 1). The first submodel is a refined version of the "*water flow and*

storage" model, which describes stem hydraulic functioning (Steppe *et al.*, 2006, 2008). Here, the transpiration demand creates a water potential gradient ($\Delta\Psi$) along the xylem that results in a radial $\Delta\Psi$ between xylem and outer tissues. This gradient pulls water from the outer tissues to the xylem to fulfill transpiration needs resulting in stem shrinkage. The opposite flow occurs when transpiration decreases and stem water reservoirs are replenished resulting in stem swelling. This submodel differentiates the osmotic and turgor pressure components of Ψ in outer tissues. When turgor is higher than a threshold value for irreversible plastic growth, stem growth occurs. Otherwise, stem diameter variations are uniquely ascribed to elastic fluctuations due to changes in water content. Stem plastic growth is a driver of the second submodel "*CO_2 sources and fluxes*". The theoretical framework of the GMRP states that respiration is partitioned into two components: (i) Growth respiration is directly related to stem growth rates. (ii) Maintenance respiration occurs in both xylem and outer tissues, is temperature-dependent according to Arrhenius kinetics, and scales with N content of the living/respiring tissues (including parenchyma in xylem). The submodel further accounts for radial CO_2 diffusion through the xylem and outer tissues, xylem CO_2 transport through the xylem, and CO_2 storage in both compartments. Finally, the third submodel "*stem carbon balance*" quantifies C sources and sinks to close the C balance at the organ level. See Table 1 and 2 for the description, acronym, and unit of model variables and parameters, respectively.

Water flow and storage submodel ("submodel A"). It is based on the original model of stem hydraulic functioning (Steppe *et al.*, 2006, 2008) with two main refinements: (i) thickness of the outer tissues compartment is represented by a linear relationship derived from simultaneous measurements of xylem and stem diameter variations (ΔD) instead of a non-linear allometric relationship (cf. Génard *et al.*, 2001); and (ii) elastic osmotically driven changes are added to elastic-tension driven and inelastic growth changes to estimate diameter stem variations (Mencuccini *et al.*, 2013, 2017; Chan *et al.*, 2016). Note that the theoretical background and mathematical development of this submodel are explained elsewhere and uniquely model refinements are explained in detail here.

Root water potential (Ψ_{ROOT}, MPa) is estimated from soil water potential (Ψ_{SOIL}, MPa):

$$\Psi_{ROOT} = \Psi_{SOIL} + D_{SOIL} \quad \text{Eqn 1}$$

where D_{SOIL} (MPa) accounts for the disequilibrium between Ψ_{SOIL} and predawn Ψ_{ROOT}. Water exchange between the xylem and outer tissues (f_{OT}, g h^{-1}) is the time derivative of the water content in outer tissues (W_{OT}, g), which is estimated from Ohm's law considering that sap flow through the xylem (SF, g h^{-1}) results from the combination of f_{OT} and root water uptake (F_{SOIL}, g h^{-1}) (cf. Eqn 9 in Steppe *et al.*, 2006):

$$\frac{dW_{OT}}{dt} = \frac{\Psi_{ROOT} - \Psi_{OT} - (SF\ R_{XY})}{R_{XY} + R_{OT}} \quad \text{Eqn 2}$$

$$f_{OT} = \frac{dW_{OT}}{dt} \quad \text{Eqn 3}$$

where Ψ_{OT} (MPa) is Ψ in outer tissues, R_{XY} (MPa h g^{-1}) is the xylem axial resistance to water flow, and R_{OT} (MPa h g^{-1}) is the radial resistance to water exchange between xylem and outer tissues. Stem hydraulic capacitance of the outer tissues (C_{OT}, g MPa^{-1}) is defined by the ratio between W_{OT} and Ψ_{OT}, and the time derivative of Ψ_{OT} is estimated as follows:

$$\frac{d\Psi_{OT}}{dt} = \frac{f_{OT}}{C_{OT}} \quad \text{Eqn 4}$$

Xylem water potential (Ψ_{XY}, MPa) is given by:

$$\Psi_{XY} = f_{OT}\ R_{OT} + \Psi_{OT} \quad \text{Eqn 5}$$

and F_{SOIL} is calculated from Ohm's law:

$$F_{SOIL} = \frac{\Psi_{ROOT} - \Psi_{XY}}{R_{XY}} \quad \text{Eqn 6}$$

Changes in W_{OT} are linked to the turgor pressure of outer tissues (Ψ_{OT}^{P}, MPa):

$$\frac{d\psi_{OT}^{P}}{dt} = \frac{dW_{OT}}{dt}\ \frac{\varepsilon}{\rho_W\ V_{OT}} \quad \text{Eqn 7}$$

where ρ_W (g m^{-3}) is water density, V_{OT} (m^3) is the volume of the outer tissues compartment, and ε (MPa) is the bulk elastic modulus of outer tissues in relation to reversible dimensional changes, which is proportional to stem diameter (D, m) and Ψ_{OT}^{P}:

$$\varepsilon = \varepsilon_0\ D\ \psi_{OT}^{P} \quad \text{Eqn 8}$$

where ε_0 (m^{-1}) is the proportionality constant. Assuming the thickness of the outer tissues (d_{OT}, m) is much smaller than the xylem diameter (D_{XY}, m), volume of outer tissues (V_{OT}) is estimated as:

$$V_{OT} = \pi\ d_{OT}\ D_{XY}\ L \quad \text{Eqn 9}$$

where L (m) is the length of the stem segment. The osmotic pressure in the outer tissues (Ψ_{OT}^{O}, MPa) is the difference between Ψ_{OT}^{P} and Ψ_{OT}; and their time derivatives are estimated likewise:

$$\frac{d\psi_{OT}^{O}}{dt} = \frac{d\psi_{OT}^{P}}{dt} - \frac{d\Psi_{OT}}{dt} \quad \text{Eqn 10}$$

Temporal changes in stem diameter (dD/dt, m h^{-1}) are calculated as the additive effect of irreversible plastic growth (dD_P/dt, m h^{-1}), elastic tension-driven (dD_{ET}/dt, m h^{-1}) and elastic osmotically-driven (dD_{EO}/dt, m h^{-1}) changes in water content of outer tissues (Chan *et al.*, 2016; Mencuccini *et al.*, 2017).

$$\frac{dD}{dt} = \frac{dD_P}{dt} + \frac{dD_{ET}}{dt} + \frac{dD_{EO}}{dt} \quad \text{Eqn 11}$$

When Ψ_{OT}^{P} exceeds a threshold value for cell growth (Γ, MPa), irreversible plastic cell growth occurs (cf. Eqns 28 and 29 in Steppe *et al.*, 2006):

$$\frac{dD_P}{dt} = \frac{d_{OT}\ \Phi}{k_d}\ (\psi_{OT}^{P}\ -\ \Gamma) \qquad \text{when } \Psi_{OT}^{P} > \Gamma \quad \text{Eqn 12}$$

$$\frac{dD_P}{dt} = 0 \qquad \text{when } \Psi_{OT}^{P} \leq \Gamma \quad \text{Eqn 13}$$

where Φ (MPa^{-1} h^{-1}) is the extensibility of cell walls in relation to non-reversible dimensional changes, and k_d (m m^{-1}) represents the contribution of changes in thickness of outer tissues (d_{OT}) relative to changes in total stem diameter (dd_{OT}/dD). Therefore:

$$\frac{dd_{OT}}{dt} = k_d\ \frac{dD}{dt} \quad \text{Eqn 14}$$

Changes in d_{OT} are assumed to be proportional to those in stem diameter (D). Measurements with two point dendrometers located at the bark and the xylem showed that this linear fit optimized d_{OT} simulation (Fig. S1), previously described by a non-linear fit following Génard *et al.* (2001). Note that for large trees, this relationship could deviate from a linear one and could be refined by analyzing measurements with two point dendrometers as indicated above. The allometric non-linear fit was uniquely applied to estimate initial d_{OT} (Fig. S2).

Elastic tension-driven changes in stem D (dD_{ET}/dt) are derived from Hooke´s law and given by (cf. Eqn 24 in Steppe *et al.*, 2006):

$$\frac{dD_{ET}}{dt} = \frac{2\ d_{OT}}{\varepsilon}\ \frac{d\psi_{OT}^{P}}{dt} \quad \text{Eqn 15}$$

Osmotically-driven changes in water content (Mencuccini *et al.*, 2013) of outer tissues uniquely result from fluctuations in the concentration of carbohydrates because tension-driven changes are calculated independently. Hence, for a constant Ψ_{OT} ($d\Psi_{OT}/dt = 0$), any change in the osmotic component of Ψ_{OT} is compensated by an equal change of the pressure component in absolute terms (Eqn S13 in Mencuccini *et al.*, 2017). In this way, osmotically-driven changes in stem D (dD_{EO}/dt) can be estimated applying Hooke´s law (cf. Eqn S14 in Mencuccini *et al.*, 2017) likewise tension-driven changes (dD_{ET}/dt) are estimated:

$$\frac{dD_{EO}}{dt} = \frac{2\, d_{OT}}{\varepsilon}\, \frac{d\psi_{OT}^{O}}{dt} \qquad \text{Eqn 16}$$

Finally, the time derivative of D_{XY} is estimated according to the geometry of the stem:

$$\frac{dD_{XY}}{dt} = \frac{dD}{dt} - 2\, \frac{dd_{OT}}{dt} \qquad \text{Eqn 17}$$

CO_2 sources and fluxes submodel ("submodel B"). Growth and respiratory fluxes are expressed in moles of C and CO_2, respectively, and on a stem volume basis accounting for the relative portion of xylem and outer tissues. Once plastic variation in stem diameter (dD_P/dt) is separated from elastic fluctuations, stem growth (G, mol C m^{-3} h^{-1}) is calculated as the time derivative of new biomass added to the stem. For this, new biomass is estimated as the product of new volume by its density, and new volume is derived with respect to D_P assuming a cylindrical geometry of the stem (see Note S1a for details):

$$G = \frac{D_P}{D^2}\, \frac{dD_P}{dt}\, (\rho_{OT} + \rho_{XY})\, \frac{C_C}{M_C} \qquad \text{Eqn 18}$$

where ρ_{OT} and ρ_{XY} (g m^{-3}) is density of the outer tissues and xylem, respectively, C_C (g C g^{-1}) is stem C content and M_C (g mol^{-1}) is C molar mass. Note that the initial value of D_P is assumed equal to that of D_{XY}, and plastic growth accounts for cambial differentiation into both xylem and outer tissues cells (even if growth is assumed to uniquely occur in the outer tissues compartment to keep assumptions from submodel A valid). According to the GMRP, growth respiration (R_G, mol CO_2 m^{-3} h^{-1}) is estimated as a function of G and the growth yield (Y_G, mol C mol C^{-1}), defined as the ratio between new structural matter added to the stem and the amount of assimilates required for it (Amthor, 2000):

$$R_G = G\, \frac{1}{1 + Y_G} \qquad \text{Eqn 19}$$

Maintenance respiration (R_M, mol CO_2 m^{-3} h^{-1}) is sensitive to temperature (Amthor, 2000; Tjoelker *et al.*, 2001) and is estimated on a N content basis (Ryan, 1991; Reich *et al.*, 2008). Total R_M is allocated into xylem and outer tissues compartments ($R_M = R_{M\_XY} + R_{M\_OT}$) according to their corresponding N concentration ([N], g N g^{-1}), and accounting for stem allometry (see Note S1b for details):

$$R_{M\_XY} = R_{b\_N}\,[\mathrm{N}]_{XY}\,\frac{\rho_{XY}}{M_N}\,Q_{10}^{\frac{T-T_b}{10}}\frac{V_{XY}}{V_S} \qquad \text{Eqn 20}$$

$$R_{M\_OT} = R_{b\_N}\,[\mathrm{N}]_{OT}\,\frac{\rho_{OT}}{M_N}\,Q_{10}^{\frac{T-T_b}{10}}\frac{V_S-V_{XY}}{V_S} \qquad \text{Eqn 21}$$

where R_{b_N} (mol CO_2 mol N^{-1} h^{-1}) is respiration at basal temperature (T_b, ºC) on a N molar basis, M_N (g mol^{-1}) is the molar mass of N, Q_{10} is the temperature sensitivity of R_M, T is the stem temperature, and V_{XY} and V_S (m^3) are the volume of the xylem and the stem within the monitored segment (considering the length L_S (m) of the monitored segment). Average values of [N] across cell tissues in both xylem and outer tissues are considered to represent R_M on a volume basis without distinction among cell tissues. Note that in this study case there was no heartwood (see ´Measurements and plant material´) and the whole xylem compartment was assumed to respire. To apply TReSpire in mature trees with heartwood, a third coaxial cylinder should be added into the stem structure to account for stem allometry while differentiating between living/respiring compartments (xylem and outer tissues) and non-respiring ones (heartwood).

Stem respiration (R_S, mol CO_2 m^{-3} h^{-1}) is the sum of the growth and maintenance components:

$$R_S = R_G + R_M = R_G + R_{M\_XY} + R_{M\_OT} \qquad \text{Eqn 22}$$

Once total R_S is known, CO_2 solubility in xylem sap and radial CO_2 diffusivity are calculated. According to Henry´s law, the concentration of CO_2 dissolved in sap solution ([CO_2^*], mol CO_2 L^{-1}) is proportional to the partial pressure of CO_2 in the gas phase in the xylem (pCO_2, atm) (Hari *et al.*, 1991; Levy *et al.*, 1999; McGuire & Teskey, 2002; Hölttä & Kolari, 2009):

$$[CO_2^*] = k_H\left(1 + \frac{k_1}{10^{-pH}} + \frac{k_1 k_2}{(10^{-pH})^2}\right) pCO_2 \qquad \text{Eqn 23}$$

where k_H (mol atm^{-1} L^{-1}), k_1 and k_2 are temperature-dependent solubility coefficients for CO_2 in water (see Note S1c for details), and pH is sap pH. Assuming ideal behavior, xylem CO_2 concentration in the gas phase ($[CO_2]_{XY}$, mol CO_2 m^{-3}) is:

$$[CO_2]_{XY} = \frac{pCO_2}{R\,T} = \frac{[CO_2^*]}{k_H\left(1+\frac{k_1}{10^{-pH}}+\frac{k_1 k_2}{(10^{-pH})^2}\right)}\,\frac{1}{R\,T} \quad \text{Eqn 24}$$

where R (m^3 atm K^{-1} mol^{-1}) is the ideal gas constant and T (K) is stem temperature. Note that the * superscript refers to the liquid phase to differentiate from the gas phase.

The mass balance approach (MBA) proposed by McGuire & Teskey (2004) calculates R_S as the sum of stem CO_2 efflux, xylem CO_2 transport, and the storage flux. Here, we refine the MBA by taking into account the geometry and the spatial location of different compartments proposed in TReSpire. To this end, two parallel mass balances in xylem and outer tissues are simultaneously applied to estimate R_S. Respired CO_2 in each compartment is the sum of the corresponding R_M (R_{M_XY} or R_{M_OT}) and half of R_G, assuming that CO_2 derived from the synthesis of new tissues in the cambium layer equally diffuses to the xylem and outer tissues following periclinal division of cambial cells. In this way, half of R_G radially diffuses to the xylem (Eqn 25), and the second half of R_G to the outer tissues (Eqn 26). Additionally, storage flux integrates CO_2 build-up in both gas and liquid phases (ΔS and ΔS^*, respectively) (cf. McGuire & Teskey, 2004). In this way, the mass balance in the xylem is given by:

$$R_{M\_XY} + \frac{R_G}{2} = E_{XY} + F_T + (\Delta S_{XY} + \Delta S^*_{XY}) \quad \text{Eqn 25}$$

where E_{XY} (mol CO_2 m^{-3} h^{-1}) is CO_2 efflux from xylem to outer tissues, F_T (mol CO_2 m^{-3} h^{-1}) is axial CO_2 flux through the xylem, ΔS_{XY} (mol CO_2 m^{-3} h^{-1}) and ΔS^*_{XY} (mol CO_2 m^{-3} h^{-1}) is the storage flux in the xylem in gas and liquid phase, respectively. Similarly, the mass balance in outer tissues is given by:

$$R_{M\_OT} + \frac{R_G}{2} = (E_A - E_{XY}) + \Delta S_{OT} \quad \text{Eqn 26}$$

where E_A (mol CO_2 m^{-3} h^{-1}) is the CO_2 efflux from outer tissues to the atmosphere, and ΔS_{OT} (mol CO_2 m^{-3} h^{-1}) is the storage flux in outer tissues in the gas phase. Note that F_T and ΔS^* in outer tissues are neglected for model simplicity due to the small V_{OT} relative to V_S (d_{OT} < 5% of D; Fig S2), fraction directly related to the magnitude of these fluxes (see eqns below).

Radial E_{XY} and E_A follows Fick´s law of diffusion. According to the geometry of the xylem and outer tissues (see Note S1d for details):

$$E_{XY} = \text{Dif}\,\frac{[CO_2]_{XY} - [CO_2]_{OT}}{\frac{2D_{XY}}{3\pi}}\,\frac{A_{XY}}{V_S} \quad \text{Eqn 27}$$

$$E_A = \text{Dif}\ \frac{[CO_2]_{OT} - [CO_2]_{ATM}}{\frac{d_{OT}}{2}}\ \frac{A_S}{V_S} \quad \text{Eqn 28}$$

where Dif ($m^2\ h^{-1}$) is diffusivity, $[CO_2]_{XY}$, $[CO_2]_{OT}$ and, $[CO_2]_{ATM}$ are the gaseous $[CO_2]$ (mol CO_2 m^{-3}) in xylem, outer tissues and atmosphere, respectively, and A_{XY} and A_S are the axial surface (m^2) of xylem and stem within the monitored stem segment, respectively. Given that CO_2 diffusion is ~ 10^4 faster in air than in water (Nobel, 1999), diffusivity is exponentially related to the volumetric gas fraction in the stem (VGF, $m^3\ m^{-3}$) (Sorz & Hietz, 2006):

$$Dif = \text{Dif}_0\ e^{Dif_e\ \text{VGF}} \quad \text{Eqn 29}$$

where Dif_0 ($m^2\ h^{-1}$) is diffusivity at zero VGF and Dif_e determines the shape of the exponential increase. Stem volume can be fractioned into gas, water and cell wall (VGF, VWF and VC_WF, respectively, $m^3\ m^{-3}$) (Gartner *et al.*, 2004). Assuming constant VC_WF, VGF is expected to increase to the detriment of VWF and *vice versa*:

$$VGF = (1 - \text{VWF} - \text{VC}_W\text{F}) \quad \text{Eqn 30}$$

and variation in VWF is assumed to be proportional to that in W_{OT} (from submodel A):

$$VWF = \text{VWF}_{t0}\ (1 - \frac{(W_{OT})_{t0} - W_{OT}}{(W_{OT})_{t0}}) \quad \text{Eqn 31}$$

where VWF_{t0} and $(W_{OT})_{t0}$ is the initial VWC and the initial water content in outer tissues, respectively. For model simplicity and to avoid over-parameterization, VGF and Dif are assumed equal in xylem and outer tissues.

Xylem CO_2 transport (F_T) is calculated following McGuire & Teskey (2004):

$$F_T = \text{SF}\ \Delta[CO_2^*]\ \frac{1}{V_S} \quad \text{Eqn 32}$$

where SF is sap flow ($m^3\ h^{-1}$) and $\Delta[CO_2^*]$ (mol CO_2 m^{-3}) is the vertical gradient in $[CO_2^*]$ along the monitored stem segment. Note F_T is expressed on a stem volume basis (cf. McGuire & Teskey, 2004; see Note S1e for details). Given that $\Delta[CO_2^*]$ is rarely constant and can be altered by e.g. transpiration and respiratory rates, it is allowed to vary with time in a linear manner:

$$\frac{\text{d}\Delta[CO_2^*]}{dt} = \Delta[CO_2^*]_{slope} \quad \text{Eqn 33}$$

where $\Delta[CO_2^*]_{slope}$ (mol CO_2 $m^{-3}\ h^{-1}$) represents the slope of the variation of $\Delta[CO_2^*]$ with time.

To close the mass balance in outer tissues, ΔS_{OT} is calculated once all other terms in Eqn 26 are known. The time derivative of $[CO_2]_{OT}$ is estimated, by definition (McGuire & Teskey, 2004), as follows:

$$\frac{d[CO_2]_{OT}}{dt} = \Delta S_{OT} \frac{1}{VGF} \quad \text{Eqn 34}$$

Similarly, ΔS_{XY} is estimated as a function of the time derivative of $[CO_2]_{XY}$:

$$\Delta S_{XY} = \frac{d[CO_2]_{XY}}{dt} VGF \quad \text{Eqn 35}$$

Finally, ΔS^*_{XY} is calculated once all other terms in Eqn 25 terms are known, and it equals the time derivative of $[CO_2^*]$ accounting for the amount of water in the stem segment:

$$\frac{d[CO_2^*]}{dt} = \Delta S^*_{XY} \frac{1}{VWF\ \rho_W} \quad \text{Eqn 36}$$

where ρ_W is water density.

Stem C balance ("submodel C"). Phloem unloading, sugar-starch interconversion, growth, respiration and osmoregulation, expressed in sucrose equivalents and on a stem volume basis (g sucrose h^{-1} m^{-3}) are quantified to close the stem C balance (Lacointe & Minchin, 2008; De Schepper & Steppe, 2010).

Phloem unloading (U) is derived from the vertical gradient in turgor pressure of phloem cells along the stem by means of monitoring stem D variations (ΔD) across the stem length (Sevanto *et al.*, 2014) (i.e., at the stem base and at the upper stem just below the first branch in this study). The first part of submodel A (Eqns. 1-6, the so-called "water transport submodel" in Steppe *et al.* (2006, 2008)), is assumed to behave equally along the vertical gradient, and the second part of submodel A (Eqns. 7-17, the so-called "stem diameter variation submodel" in Steppe *et al.* (2006, 2008)) is calibrated and run for a second time according to ΔD in the upper part of the stem (D_{UP}). Note that submodel A is calibrated against stem ΔD at the stem base (see "Measurements and plant material"), and to avoid model over-parameterization, parameters applied and calibrated for the lower part of the stem are assumed to remain constant along the vertical gradient. Likewise, measured and simulated variables included in Eqns. 1-6 determining axial and radial water flows (SF, f_{OT}, Ψ_{XY} and Ψ_{OT}) are assumed to be the same in the lower and upper stem, and variables from which D_{UP} is estimated (Eqns. 7-17; ε_{UP}, V_{OT_UP}, $\Psi_{OT\_UP}^{O}$, $\Psi_{OT\_UP}^{P}$, D_{XY_UP}, d_{OT_UP}, D_{P_UP}, dD_{ET_UP} and dD_{EO_UP}) are simulated for a second time for the upper part of the stem. In this way, the osmotic

and pressure components of Ψ_{OT} do change with stem height, and the pressure drop along the stem ($\Delta\Psi_{OT}^{P}$, MPa) is given by the difference between Ψ_{OT}^{P} (MPa) in the upper and lower stem accounting for the gravitational pressure difference (Hölttä *et al.*, 2009):

$$\Delta\Psi_{OT}^{P} = \left(\Psi_{OT\_UP}^{P} - \Psi_{OT}^{P}\right) + (\rho_w \, g \, L) \quad \text{Eqn 37}$$

where g (MPa m^2 g^{-1}) is the gravitational constant. Note that the subscript for the lower part of the stem is omitted for consistency with the terminology proposed in submodel A. According to Münch theory, variations in the pressure component of Ψ_{OT} along the stem are driven by variations in the osmotic component due to loading-unloading phloem dynamics (De Schepper & Steppe, 2010). Therefore, for a given Ψ_{OT}, the vertical drop in Ψ_{OT}^{P} equals that of Ψ_{OT}^{O} ($\Delta\Psi_{OT}^{P} = \Delta\Psi_{OT}^{O}$), and the vertical gradient in sucrose concentration in outer tissues along the stem ($\Delta[SU]_{OT}$, g m^{-3}) can be estimated with the van´t Hoff equation (see Note S1f for details):

$$\Delta[SU]_{OT} = \frac{\Delta\Psi_{OT}^{P} \, M_{SU}}{R \, T} \quad \text{Eqn 38}$$

where M_{SU} (g mol^{-1}) is the molar mass of sucrose, R (m^3 MPa K^{-1} mol^{-1}) is the universal gas constant and T (K) is temperature. Single phase Michaelis-Menten kinetics describe U (g m^{-3} h^{-1}) rates (Minchin & Lacointe, 2017) (see Note S1g for details):

$$U = \frac{V_{max} \, M_{SU} \, \Delta[SU]_{OT}}{k_M \, M_{SU} + \Delta[SU]_{OT}} \quad \text{Eqn 39}$$

where V_{max} (mol m^{-3} h^{-1}) and k_M (mol m^{-3}) are kinetic parameters.

The time derivative of starch concentration ([ST], g m^{-3}) is determined by a constant target concentration of sucrose ($[SU]_{targ}$, g m^{-3}) in the outer tissues (Lacointe & Minchin, 2008; De Schepper & Steppe, 2010):

$$\frac{d[ST]}{dt} = k_{starch} \left([SU] - [SU]_{targ}\right) \quad \text{Eqn 40}$$

where [SU] is the sucrose concentration in outer tissues and k_{starch} (h^{-1}) is a kinetic parameter. When [SU] (g m^{-3}) is higher than $[SU]_{targ}$, starch is synthesized and *vice versa*, so that starch synthesis and depolymerization are given by positive and negative values, respectively. For calibration purposes, starch storage is assumed to occur in the xylem. Sugar-starch interconversion (SSI, g m^{-3} h^{-1}) is therefore given by:

$$SSI = \frac{d[ST]}{dt} \, \frac{V_{XY}}{V_S} \quad \text{Eqn 41}$$

Stem growth and respiration sinks (G_{SU} and R_{S_SU}, g m^{-3} h^{-1}, respectively; in sucrose equivalents) are quantified as follows:

$$G_{SU} = G\frac{M_{SU}}{12} \quad \text{Eqn 42}$$

$$R_{S\_SU} = R_S\frac{M_{SU}}{12} \quad \text{Eqn 43}$$

with 12 being the ratio of C (or CO_2) mol to sucrose ($C_{12}H_{22}O_{11}$) mol.

In this case study, woody tissue photosynthesis was disabled (see "Measurements and plant material") and hence neglected for modelling purposes. Finally, the time derivative of [SU] in outer tissues is given by:

$$\frac{d[SU]}{dt} = (U - G_{SU} - R_{S\_SU} - SSI)\frac{V_S}{V_S - V_{XY}} \quad \text{Eqn 44}$$

where $V_S/(V_S\text{-}V_{XY})$ accounts for stem allometry assuming that osmoregulation (OR = d[SU]/dt, g m^{-3} h^{-1}) uniquely occurs in the outer tissues compartment given that the osmotic component of Ψ_{XY} is zero (Steppe *et al.*, 2006).

Measurements and plant material

To run and calibrate TReSpire, an array of variables should be measured (Table 3). Briefly, sap flow and soil water potential are used as inputs in submodel A, which is calibrated against stem ΔD and xylem water potential. Submodel B is driven by previous model outputs and stem temperature, and is calibrated against E_A. Submodel C in turn is driven by previous model outputs and calibrated against stem ΔD at the upper part of the stem and concentrations of soluble sugars and starch. Additionally, some stem features included in TReSpire as parameters were measured or estimated from ancillary trees (see below). These include L, initial D, k_d, ρ_{XY}, ρ_{OT}, [N] and [C] in xylem and outer tissues, and sap pH (Table S1). See Methods S1 for a detailed explanation of sensors and methods applied to measure abovementioned variables and parameters, and Methods S2 for a picture of the experiment setup.

To present TReSpire, data from a monitored Norway maple tree (*Acer platanoides* L. ´Crimson King´) during the growing season in spring (DOYs 155-160) is shown. Data was collected in 2017 within the context of a larger experiment to evaluate TReSpire across different species, phenological stages and under drought stress conditions. In this larger experiment, ancillary trees of the same species, age, size, and grown under identical conditions were instrumented to monitor

xylem [CO_2] and xylem ΔD with intrusive methods to be avoided in modelling-dedicated trees. Data from ancillary trees is also presented here for model validation. Trees were grown outdoors in a plant nursery and transported to the glasshouse facilities of Ghent University prior to measurements. Maple trees averaged 4 cm in diameter at 1 m height, 315 cm in total height and 180 cm of stem length before the first branch.

Model implementation and analyses

Model simulation, calibration, sensitivity and identifiability analyses were performed using the plant modelling software PhytoSim (version 2.1, Phyto-IT, Gent, Belgium). Simulations started at nighttime before transpiration resumes, assuming hydraulic equilibrium along the root-to-leaf continuum. Simulations were performed with a fourth-order variable step size solver with an accuracy of 10^{-6} and a maximum step size of 0.1 h. Model parameterization was performed by applying the Simplex optimization method (Nelder & Mead, 1965) in order to minimize the weighted sum of squared errors between data and model simulation. Prior to model parameterization, an identifiability analysis was performed to select an identifiable parameter subset following the procedure described in De Pauw *et al.* (2008). In order for a parameter subset to be identifiable from the available data, two conditions need to be met: (1) the subset needs to be as sensitive as possible and (2) the correlations between the parameters of the subset need to be as low as possible (low collinearity). The remaining unidentifiable parameters were assigned values based on literature or previous modelling exercises (see Table S1 for further details). For the estimated parameters, 95% confidence intervals and relative standard errors were calculated based on the parameter estimation covariance matrix (Steppe *et al.*, 2006). The parameter estimation covariance matrix was calculated using a two-step procedure. First, it was calculated for the estimated parameters of submodels A and B, then it was calculated for the parameters of submodel C. This was done to avoid numerical errors which arose when calculating the matrix for the entire estimated parameter subset. The poor identifiability of parameters in submodel C caused the entire matrix to become near-singular, which is known to cause problems when trying to invert it. Although we were not able to obtain a parameter estimation error for submodel C, the estimated values itself were realistic and did not cause problems when running the model.

Results

Table 4 shows the largest subset of identifiable parameters of submodels A and B with highest sensitivity index (R_{XY}, R_{OT}, C_{OT}, Φ, Y_G, R_{b_N}, Q_{10}, Dif_e and $\Delta[CO_2^*]_{slope}$), which was calibrated with a relative standard error ≤ 2%. Due to a high collinearity between Dif_e and Dif_0 and between C_{OT} and ε_0, parameters Dif_0 and ε_0 were not included in the calibration and values from literature or preliminary calibrations were applied (Table S1). Initial values of derivative variables $[CO_2^*]$, $[CO_2^*]_{OT}$ and $\Delta[CO_2^*]$ were also identifiable. Ψ_{XY} was highly sensitive to R_{XY}, stem D to Φ, and E_A to both Dif_e and Y_G, followed by R_{b_N} and Q_{10}. Some parameter subsets from submodel C showed high collinearities (e.g. between V_{max} and K_M, and between k_{starch} and $[SU]_{targ}$). Therefore, only the subset of parameters constituted by V_{max} and k_{starch} and the initial value of $\Psi_{OT}{}^{P}{}_{UP}$ were calibrated (Table S1), while K_M, $[SU]_{targ}$ and the initial values of [SU] and [ST] were taken from literature or using expert knowledge (Table S1). See Table S2 for the sensitivity analysis of submodel C.

Submodel A accurately simulated stem D variations and Ψ_{XY} (Fig. 2). Three sources of fluctuations in stem D were disentangled. Driven by turgor pressure, irreversible plastic growth (dD_P/dt) occurred throughout the sub-daily period with higher rates at nighttime. Elastic tension-driven changes (dD_{ET}/dt) caused substantial daytime shrinkage and nighttime swelling, while osmotically-driven changes (dD_{EO}/dt) were comparatively much smaller and exhibited the opposite pattern (Fig. 2a). Ψ_{OT} lagged behind Ψ_{XY} and its pressure component fluctuated more than the osmotic counterpart (Fig. 2b).

Stem respiration fluctuated between 1.1 and 2.2 mol CO_2 m^{-3} h^{-1} and was partitioned into R_G, R_{M_OT} and R_{M_XY} (Fig. 3a). R_G mimicked dD_P/dt sub-daily dynamics, with highest rates at nighttime up to 0.5 mol CO_2 m^3 h^{-1}. On the other hand, R_M in xylem and outer tissues were temperature dependent and exhibited highest rates during daytime, with R_{M_XY} being higher than R_{M_OT}. Simulated E_A fluctuated between 1.0 and 1.9 mol CO_2 m^{-3} h^{-1}, accounting for most of R_S (Fig. 3b). Daytime E_A was accurately simulated, whereas nighttime E_A was slightly overestimated. F_T was the second largest component of R_S and was driven by sap flow dynamics. F_T reached an initial peak of 1.1 mol CO_2 m^{-3} h^{-1}, and progressively decreased to a sub-daily maximum of 0.2 mol CO_2 m^{-3} h^{-1} following a reduction in the vertical gradient of sap $[CO_2^*]$ across the surveyed period ($\Delta[CO_2^*]_{slope}$ = -5.8×10^{-3} mol CO_2 m^{-3} h^{-1}). Storage fluxes were the smallest component of R_S, with xylem storage in both liquid (ΔS^*_{XY}) and gaseous (ΔS_{XY}) phase accounting for most of it, while

462 CO_2 storage in outer tissues (ΔS_{OT}) was negligible. CO_2 was stored at nighttime and released at
463 daytime.

464 Submodel B yielded additional insights in R_S and related respiratory fluxes (Fig. 4). Maintenance
465 respiration (integrating xylem and outer tissues) roughly accounted for 55-85% of total R_S, with
466 R_{M_XY} contributing with 35-55% to R_S. E_A accounted for 85-95% of R_S at nighttime, with minimum
467 values down to 70% during daytime (Fig. 4a). Xylem CO_2 concentration in the gas and liquid phase
468 ranged between 2.0 and 4.9 mol m^{-3}, and between 2.5 and 6.8 mmol L^{-1}, respectively (Fig. 4b);
469 values consistent with measurements performed in ancillary trees (Fig S3a, S3c). In outer tissues,
470 $[CO_2]$ was substantially lower (0.3-0.6 mol m^{-3}). Sub-daily dynamics in $[CO_2^*]$, $[CO_2]_{XY}$ and
471 $[CO_2]_{OT}$ were opposite to those of stem temperature (cf. Fig S3) according to Henry´s and ideal gas
472 laws. Radial CO_2 diffusivity fluctuated between 5×10^{-9} at nighttime and 9×10^{-9} m^2 s^{-1} at daytime
473 (Fig. 4c), which was driven by transpiration dynamics and the resulting volumetric gas fraction.

474 The stem C balance (submodel C) was closed by assigning values from literature to unidentifiable
475 parameters (Table S1). Model fit of stem ΔD in the upper part stem (Fig. 5a) was worse than that
476 at the stem base (cf. Fig. 2a). Both Ψ_{OT}^P and Ψ_{OT}^O were higher (in absolute terms) in the upper
477 stem resulting in a vertical pressure gradient fluctuating between 0.1 and 0.2 MPa (Fig. 5b). Across
478 the surveyed period, [SU] was roughly stable and below $[SU]_{targ}$ resulting in a progressive reduction
479 of [ST] by means of starch depolymerization (Fig. 5c). Phloem unloading (76-89 g m^{-3} h^{-1}) and
480 starch depolymerization (10-11 g m^{-3} h^{-1}) fuelled growth (38-70 g m^{-3} h^{-1}) and respiration (32-63 g
481 m^{-3} h^{-1}). Mismatch between C sources and sinks were compensated for by osmoregulation (defined
482 as the time derivative of [SU]), which fluctuated between -16 and 11 g m^{-3} h^{-1} (Fig. 5d), thus acting
483 as a C sink or source according to C metabolic requirements.

484 **Discussion**

485 Submodels A and B were calibrated with high level of statistical confidence (Table 4) and were
486 useful to qualitatively and quantitatively describe stem respiration. Submodel A was pivotal to
487 simulate turgor pressure and separate plastic stem growth from elastic fluctuations, and
488 subsequently discriminate between growth and maintenance respiration on a sub-daily basis. In
489 this way, TReSpire was calibrated against stem diameter variations and stem CO_2 efflux, and hence
490 from a sink-driven perspective (Fatichi *et al.*, 2014, 2019; Steppe *et al.*, 2015). Submodel B was
491 useful to determine key parameters described by the GMRP to estimate whole plant respiration

(Y_G, Q_{10}, and R_{b_N}), and realistically simulated dynamics of CO_2 diffusion across the stem and CO_2 solubility in the sap solution, a crucial step to deepen our understanding of stem CO_2 fluxes (Teskey *et al.*, 2008, 2017; Trumbore *et al.*, 2013). On the other hand, submodel C was practical to conceptually describe C sources and sinks at the organ level; however, refinement would be necessary before gained insights from this submodel are extrapolated to large-scale models, as collinearity issues could lead to misestimation of phloem unloading and sugar-starch interconversion rates. In any case, given that stem hydraulic modelling (submodel A) has been explored and discussed to a great detail in previous works (e.g. Steppe *et al.*, 2006, 2015; Hölttä *et al.*, 2009; Mencuccini *et al.*, 2017), discussion here will deliberately focus on stem respiratory physiology (submodel B) and the stem carbon balance (submodel C), which encompass the largest advance in plant modelling proposed in TReSpire.

Insights into the growth and maintenance respiration paradigm

The GMRP separates respiration into growth and maintenance components. The growth component is directly related to the growth yield (Y_G), a parameter defined by the fraction of C added to structure per unit of substrate invested in growth metabolism. This parameter indicates how expensive the synthesis of new biomass is, and is therefore related to the species ecology (Lambers & Poorter, 1992; Rodríguez-Calcerrada *et al.*, 2019). Here, Y_G at the onset of the growing period (DOYs 155-160) was 0.818 ± 0.006 (95% CI), a coefficient at the upper end of reported values (0.7-0.85; Cannell & Thornley, 2000; Amthor, 2000). This relatively high Y_G could be attributed to seasonality in growth efficiency (Steppe *et al.*, 2015). Carbon investment in cell production and enlargement peaks at the beginning of the growing season, while C investment in cell wall thickening and lignification lags behind by 25-50 days depending on the forest biome (Cuny *et al.*, 2015). Given that lignification is comparatively more C demanding, Y_G might decline progressively as the contribution of lignification to stem size increment becomes more important. It is worth noting, however, that literature comparison is not straightforward as different growth-related subprocesses taken into account (e.g. N reduction and uptake, and phloem transport) or analytical methods applied for calculation, substantially influence Y_G estimates (Cannell & Thornley, 2000; Rodríguez-Calcerrada *et al.*, 2019).

Maintenance respiration relies on two parameters (R_{b_N} and Q_{10}). Basal respiration on a N basis at 20ºC (R_{b_N}) was $9.95\times10^{-3} \pm 0.32\times10^{-3}$ mol CO_2 mol N^{-1} h^{-1}, a value strikingly close to that reported

by Ryan (1991) in a pioneering work (10.6×10^{-3} mol CO_2 mol N^{-1} h^{-1}) that inspired plant respiration modelers. Such consistency highlights once more the tight link between [N] and the amount of proteins involved in maintenance metabolism. We initially attempted to describe the R_M-N relationship with a power function following Reich *et al.* (2008). However, the intercept and slope of this log-log relationship were highly correlated and did not reduce the weighted sum of squared errors (data not shown), so that we adopted a linear approach. We suggest that the comparatively narrow range of [N] measured here in xylem and outer tissues leads to a R_M-N relationship that can be similarly described by linear and exponential shapes. Furthermore, when the R_M-N relationship was exponentially described, Y_G tended to the unit and hence $R_G \approx 0$ and $R_S \approx R_M$. Given that in Reich's *et al.* (2008) meta-analyses, respiration rates pooled R_G and R_M, we speculate that R_M-N could be linearly described, while differences between exponential and linear predictions (R_G) could be attributed to additional N required to meet growth stoichiometry. This hypothesis, however, should be better approached with dedicated experiments. On the other hand, temperature sensitivity of R_M (Q_{10}) was 2.18±0.08. This Q_{10} is within the reported range in stems (from 1 to 3, reviewed by Wang *et al.*, 2006 and Salomón *et al.*, 2017), moderately higher than the median (1.91; Wang *et al.*, 2006) and the Q_{10} value commonly used in plant and global models (2.0). Again, literature comparison is not straightforward as (i) Q_{10} decreases across the season as plants acclimate to warmer conditions (Tjoelker *et al.*, 2001; Reich *et al.*, 2016), and (ii) Q_{10} estimates can be biased by implicit hypotheses assumed in each study case. Many studies determine Q_{10} through the exponential relationship between R_S (R_G+R_M) and temperature. However, R_G is temperature independent *per se*, and uniquely indirect temperature effects on the sink demand (growth) affect associated respiratory costs (Amthor, 2000). Therefore, inclusion of R_G to estimate Q_{10} might blur the R_M-T relationship (Salomón *et al.*, 2018).

Insights into stem CO_2 fluxes

TReSpire applies a refined version of the mass balance approach (McGuire & Teskey, 2004) including a parallel mass balance in the outer tissues in addition to that in the xylem. The spatial compartmentalization of TReSpire allows to discern the origin of respired CO_2 among xylem, outer tissues and the cambium layer, while intrusive measurement techniques are avoided. Overall, the relative contribution of E_A, F_T and ΔS to R_S, gaseous [CO_2] in xylem and outer tissues, and [CO_2^*] dissolved in sap solution are consistent with observations made across a wide array of species and

environmental conditions (reviewed by Teskey *et al.*, 2008, 2017), as well as with xylem [CO_2] measurements performed in ancillary trees instrumented for model validation (Fig. S3).

Radial CO_2 movement was driven by the [CO_2] gradient across the xylem-outer tissues-atmosphere continuum according to Fick´s law of diffusion. Simulated xylem [CO_2] was approximately one and two orders of magnitude higher than that in outer tissues and the atmosphere, respectively, which is consistent with [CO_2] measurements along this gradient (reviewed by Teskey *et al.*, 2008). This gradient responds to slow radial CO_2 diffusion in woody tissues (Sorz & Hietz, 2006; Steppe *et al.*, 2007) and stem geometry. While outer tissues consist of a relatively thin superposition of cell layers peripherally located and immediately diffusing to the atmosphere, CO_2 in the thicker xylem requires more time to reach the cambium layer facilitating CO_2 build-up (Eqns 27-28). The high water status of our well-watered monitored tree, resulted in a radial CO_2 diffusivity in woody tissues ($5\text{-}9\times10^{-9}$ m^2 s^{-1}) slightly higher than that in water (1.6×10^{-9} m^2 s^{-1}), and three orders of magnitude lower than that in air (1.6×10^{-5} m^2 s^{-1}), highlighting the substantial constraint of water and cell walls to CO_2 diffusion through woody tissues. Accordingly, our limited sub-daily range of variation in diffusivity (cf. Sorz & Hietz, 2006) followed dynamics of volumetric gas fraction, as similarly observed in poplar trees under controlled conditions (Steppe *et al.*, 2007), and in field-grown oaks experiencing seasonal drought (Salomón *et al.*, 2016). To avoid model over parameterization, TReSpire assumes equal diffusivity and volumetric water fraction between compartments, which is unlikely due to differential structure and functionality of xylem and outer tissues (Steppe *et al.*, 2015). Measurements relating water content, wood anatomy and CO_2 diffusivity (e.g. Sorz & Hietz, 2006) would help to more realistically parameterize and model CO_2 diffusion through woody tissues.

Axial CO_2 transport through xylem (F_T) explained to the greatest extent the difference between R_S and E_A (Fig. 3b) and hence E_A/R_S deviation from unity (Fig. 4a). The stem apparent respiratory quotient (ARQ = CO_2 efflux / O_2 influx) is theoretically equivalent to the E_A/R_S ratio (cf. Hölttä & Kolari, 2009) assuming that stem oxygen consumption equals stem respiration. Ratios of E_A/R_S ranging between 0.7 and 1 agree with ARQs below one, consistently observed across a range of species and conditions (Angert *et al.*, 2012; Hilman *et al.*, 2018). However, sub-daily variation in E_A/R_S according to transpiration dynamics contrasts with mostly stable ARQs along the sub-daily course (Hilman *et al.*, 2018). Comparable ARQs between day and night suggests that F_T is not the only path of 'CO_2 removal', and authors suggested that enzyme phosphoenolpyruvate carboxylase

583 (PEPC) can fix locally respired CO_2 and export the resulting product via xylem and phloem flows.
584 In this line, E_A was slightly overestimated at nighttime. TReSpire assumes that F_T is restricted to
585 daytime hours following sap flow dynamics (Eqn 32). Hence, for a given R_S, reductions in E_A
586 during nighttime can be uniquely achieved by increased CO_2 storage. However, ΔS is limited at
587 some point by CO_2 saturation in sap according to equilibrium reactions, which are pH-dependent
588 (Teskey *et al.*, 2008). F_T simulated here could be considered as a lumped flow able to remove
589 locally respired CO_2 integrating (i) CO_2 dissolved in sap (McGuire & Teskey, 2004), (ii) malate
590 dissolved in sap after PEPC activity (Angert *et al.*, 2012; Hilman *et al.*, 2018), and (iii) axial CO_2
591 diffusion in the gas phase following vertical $[CO_2]$ gradients resulting from woody tissue
592 photosynthesis above and below the monitored stem segment (Saveyn *et al.*, 2008; Salomón *et al.*,
593 2019a; De Roo *et al.*, 2019). Whatever the pathway of CO_2 removal, F_T is restricted to daytime and
594 further research on the role of PEPC activity would be necessary to integrate additional
595 mechanisms of CO_2 removal at nighttime, as well as to address potential differences in sub-daily
596 patterns between E_A/R_S simulations and ARQs measurements. Furthermore, TReSpire allows
597 temporal variation in the vertical gradient of sap $[CO_2^*]$ ($\Delta[CO_2^*]$) in a linear manner (Eqn 33).
598 Highest values of $\Delta[CO_2^*]$ and hence highest F_T at the beginning of the simulation period resulted
599 in lowest E_A/R_S ratios (0.7) at this time (Fig. 4a, 3b). However, this is an oversimplification of a
600 complex interaction among several factors that influence $\Delta[CO_2^*]$, such as transpiration rates, stem
601 allometry and tapering, and respiratory activity (Hölttä & Kolari, 2009). Further research in xylem
602 $[CO_2]$ at different heights, in several species and across the season (e.g. Teskey & McGuire, 2007;
603 Salomón *et al.*, 2016) would allow to better describe $\Delta[CO_2^*]$ dynamics in mechanistic models.

604 *Stem carbon balance*

605 The stem C balance proposed in TReSpire (submodel C) reliably estimates the sink strength of
606 physiological processes involved in the synthesis of new biomass, respiratory related costs, and
607 respiratory maintenance expenditures. However, quantification of C sources remains ambiguous
608 due to high collinearity between parameters describing phloem unloading and sugar-starch
609 interconversion. Therefore, although helpful insights related to sub-daily dynamics of stem C
610 fluxes can be gained from this submodel, a more detailed description of C sources and more data
611 for calibration would be necessary aiming at solving identifiability issues: (i) A greater degree of
612 complexity to describe and calibrate phloem transport and unloading could be incorporated by
613 accounting for phloem leakage, sieve tubes properties, phloem sap viscosity, or different solutes

not limited to sucrose equivalents (Thompson & Holbrook, 2003; Hölttä *et al.*, 2009; Minchin & Lacointe, 2017). Moreover, diameter variations in the upper stem could be recalibrated allowing vertical variation in R_{XY}, R_{OT}, C_{OT} and Φ (submodel A) to more accurately estimate the vertical drop in turgor pressure. (ii) A more detailed description of SSI processes accounting for temporal dynamics in nonstructural carbohydrates (Hartmann & Trumbore, 2016) and osmoregulation (Lintunen *et al.*, 2016) would be necessary to more realistically represent starch metabolism, simplistically determined here by a target concentration of soluble sugars (Eqn 40). In this line, data on [SU] and [ST] at a finer temporal resolution (measured only once along the simulated period) would help to avoid numerical problems that arose during the estimation of the parameter covariance matrix. (iii) Finally, inclusion of woody tissue photosynthesis, intentionally impeded and neglected here to avoid interferences with E_A measurements, would help to better quantify stem C sources given its significant impact on whole-plant C budgets (Ávila *et al.*, 2014; Steppe *et al.*, 2015).

Outlook

Ideally, biophysical models should be flexible enough to incorporate knowledge at the biochemical level, while organ-level outputs could be implemented within large-scale models. Firstly, growth and respiratory costs integrated in TReSpire (Eqns 18-22) could be itemized to subprocesses and biochemical reactions described in detail elsewhere (e.g. Cannell & Thornley, 2000; Amthor, 2000) and include new biochemical knowledge. Secondly, TReSpire (submodels A & B) could improve accuracy of current estimates of whole-plant respiration at larger spatial scales in the long term, as it is the first process-based model to predict R_S independently of leaf metabolism, practice commonly applied by TBMs. As a first step, TReSpire performance should be tested across different species and biomes, during longer periods encompassing at least one growing season, and along wide gradients of environmental conditions. If model calibration and simulation exhibit robustness, TReSpire output might be considered to be transferred to large-scale models. In this line, establishment of international research networks to collect and share data on stem respiratory fluxes (CO_2 efflux and/or O_2 influx) (see Yang *et al.*, 2016) and hydraulic measurements to run and calibrate TReSpire (submodels A and B) could result in a global database of stem respiratory traits (e.g., Y_G, Q_{10}, and R_{b_N}). Such database would be useful to compare stem respiratory physiology and ecology of different species across spatial and temporal scales.

Acknowledgements

We are grateful to Philip Deman and Geert Favyts for their inestimable work to prepare the experimental setup. We also thank our lab colleagues Jonas von der Crone and Jeroen Schreel for their help during data collection, as well as three reviewers for their thoughtful comments to improve the initial version of this manuscript. This project has received funding from the FWO and the European Union's Horizon 2020 research and innovation programme under the Marie Skłodowska-Curie grant agreement no 665501 granted to R.L.S. Funding was additionally provided by the Research Foundation Flanders (FWO), research program G.0941.15N granted to K.S. and supporting the PhD work of L.D.R.

Author contributions

RLS and KS planned and designed the research. RLS, LdR and JO performed the measurements. RLS analysed data and wrote the first draft of the manuscript. DJWDP and KS contributed to the writing of the manuscript.

References

Amthor J. **2000**. The McCree–de Wit–Penning de Vries–Thornley respiration paradigms: 30 years later. *Annals of Botany* **86**: 1–20.

Angert A, Muhr J, Negron Juarez R, Alegria Muñoz W, Kraemer G, Ramirez Santillan J, Barkan E, Mazeh S, Chambers JQ, Trumbore SE. **2012**. Internal respiration of Amazon tree stems greatly exceeds external CO_2 efflux. *Biogeosciences* **9**: 4979–4991.

Armstrong AF, Logan DC, Tobin AK, O'Toole P, Atkin OK. **2006**. Heterogeneity of plant mitochondrial responses underpinning respiratory acclimation to the cold in *Arabidopsis thaliana* leaves. *Plant, Cell and Environment* **29**: 940–949.

Atkin OK, Bahar NHA, Bloomfield KJ, Griffin KL, Heskel MA, Huntingford C, de la Torre AM, Turnbull MH. **2017**. Leaf Respiration in Terrestrial Biosphere Models. In: Tcherkez G, Ghashghaie J, eds. Plant Respiration: Metabolic Fluxes and Carbon Balance. Cham: Springer International Publishing, 107–142.

Atkin OK, Meir P, Turnbull MH. **2014**. Improving representation of leaf respiration in large-scale predictive climate – vegetation models. *New Phytologist* **202**: 743–748.

Ávila E, Herrera A, Tezara W. **2014**. Contribution of stem CO_2 fixation to whole-plant carbon balance in nonsucculent species. *Photosynthetica* **52**: 3–15.

Campioli M, Malhi Y, Vicca S, Luyssaert S, Papale D, Peñuelas J, Reichstein M, Migliavacca M, Arain MA, Janssens IA. **2016**. Evaluating the convergence between eddy-covariance and biometric methods for assessing carbon budgets of forests. *Nature Communications* **7**: 13717.

Cannell MGR, Thornley JHM. **2000**. Modelling the Components of Plant Respiration: Some Guiding Principles. *Annals of Botany* **85**: 45–54.

Chan T, Hölttä T, Berninger F, Mäkinen H, Nöjd P, Mencuccini M, Nikinmaa E. **2016**. Separating water-potential induced swelling and shrinking from measured radial stem variations reveals a cambial growth and osmotic concentration signal. *Plant, Cell & Environment* **39**: 233–244.

Coussement JR, De Swaef T, Lootens P, Roldán-Ruiz I, Steppe K. **2018**. Introducing turgor-driven growth dynamics into functional-structural plant models. *Annals of Botany* **121**: 849–861.

Cuny HE, Rathgeber CBK, Frank D, Fonti P, Mäkinen H, Prislan P, Rossi S, del Castillo EM, Campelo F, Vavrčík H, *et al.* 2015. Woody biomass production lags stem-girth increase by over one month in coniferous forests. *Nature Plants* **1**: 15160.

Dietze M, Serbin S, Davidson C, Desai A, Feng X, Kelly R, Kooper R, Lebauer D, Mantooth J, Mchenry K, *et al.* 2014. A quantitative assessment of a terrestrial biosphere model's data needs across North American biomes. *Journal of Geophysical Research: Biogeosciences* **119**: 286–300.

Farquhar GD, Caemmerer S Von, Berry JA. **1980**. A biochemical model of photossynthestic CO_2 assimilation in leaves of C3 species. *Planta* **90**: 78–90.

Fatichi S, Leuzinger S, Korner C. **2014**. Moving beyond photosynthesis: from carbon source to sink-driven vegetation modeling. *New Phytologist* **201**: 1086–1095.

Fatichi S, Pappas C, Zscheischler J, Leuzinger S. **2019**. Modelling carbon sources and sinks in terrestrial vegetation. *New Phytologist* **221**: 652–668.

Gartner BL, Moore JR, Gardiner BA. **2004**. Gas in stems: Abundance and potential consequences for tree biomechanics. *Tree Physiology* **24**: 1239–1250.

Génard M, Fishman S, Vercambre G, Huguet J-G, Bussi C, Besset J, Habib R. **2001**. A biophysical analysis of stem and root diameter variations in woody plants. *Plant Physiology* **126**: 188–202.

Gifford RM. **2003**. Plant respiration in productivity models: conceptualisation, representation and issues for global terrestrial carbon-cycle research. *Functional Plant Biology* **30**: 171–186.

Hari P, Nygren P, Korpilahti E. **1991**. Internal circulation of carbon within a tree. *Canadian Journal of Forest Research* **21**: 514–515.

Hartmann H, Trumbore S. **2016**. Understanding the roles of nonstructural carbohydrates in forest trees - from what we can measure to what we want to know. *New Phytologist* **211**: 386–403.

Hilman B, Muhr J, Trumbore SE, Carbone MS, Yuval P, Joseph S. **2018**. Comparison of CO_2 and O_2 fluxes demonstrate retention of respired CO_2 in tree stems from a range of tree species. *Biogeosciences* **1**: 1–30.

Hölttä T, Kolari P. **2009**. Interpretation of stem CO_2 efflux measurements. *Tree Physiology* **29**: 1447–1456.

Hölttä T, Mencuccini M, Nikinmaa E. **2009**. Linking phloem function to structure: Analysis with a coupled xylem–phloem transport model. *Journal of Theoretical Biology* **259**: 325–337.

Lacointe A, Minchin PEH. **2008**. Modelling phloem and xylem transport within a complex architecture. *Functional Plant Biology* **35**: 772–780.

Lambers H, Poorter H. **1992**. Inherent variation in growth rate between higher plants: A search for physiological causes and ecological consequences. *Advances in Ecological Research **23**:187-261*.

Levy PE, Meir P, Allen SJ, Jarvis PG. **1999**. The effect of aqueous transport of CO_2 in xylem sap on gas exchange in woody plants. *Tree Pysiology* **19**: 53–58.

Lintunen A, Paljakka T, Jyske T, Peltoniemi M, Sterck F, von Arx G, Cochard H, Copini P, Caldeira MC, Delzon S, *et al.* 2016. Osmolality and non-structural carbohydrate composition in the secondary phloem of trees across a latitudinal gradient in Europe. *Frontiers in Plant Science* **7**: 1–15.

McGuire MA, Teskey RO. **2002**. Microelectrode technique for in situ measurement of carbon dioxide concentrations in xylem sap of trees. *Tree Physiology* **22**: 807–811.

McGuire MA, Teskey RO. **2004**. Estimating stem respiration in trees by a mass balance approach that accounts for internal and external fluxes of CO_2. *Tree Physiology* **24**: 571–578.

Meir P, Shenkin A, Disney M, Rowland L, Malhi Y, Herold M, da Costa ACL. **2017**. Plant structure-function relationships and woody tissue respiration: Upscaling to forests from laser-derived measurements. In: Tcherkez G, Ghashghaie J, eds. Plant Respiration: Metabolic fluxes and carbon balance. Cham: Springer International Publishing, 89–105.

Mencuccini M, Hölttä T, Sevanto S, Nikinmaa E. **2013**. Concurrent measurements of change in the bark and xylem diameters of trees reveal a phloem-generated turgor signal. *New Phytologist* **198**: 1143–1154.

Mencuccini M, Salmon Y, Mitchell P, Hölttä T, Choat B, Meir P, O'Grady A, Tissue D, Zweifel R, Sevanto S, *et al.* 2017. An empirical method that separates irreversible stem radial growth from bark water content changes in trees: theory and case studies. *Plant, Cell & Environment* **40**: 290–303.

Minchin PEH, Lacointe A. **2017**. Consequences of phloem pathway unloading/reloading on equilibrium flows between source and sink: a modelling approach. *Functional Plant Biology* **44**: 507-514.

Nelder JA, Mead R. **1965**. A simplex method for function minimization. *The Computer Journal* **7**: 308–313.

Nobel PS. **1999**. *Physicochemical and environmental plant physiology*. San Diego, CA, USA: Academic Press.

De Pauw DJW, Steppe K, De Baets B. **2008**. Identifiability analysis and improvement of a tree water flow and storage model. *Mathematical Biosciences* **211**: 314–332.

Reich PB, Sendall KM, Stefanski A, Wei X, Rich RL, Montgomery RA. **2016**. Boreal and temperate trees show strong acclimation of respiration to warming. *Nature* **531**: 633–636.

Reich PB, Tjoelker MG, Pregitzer KS, Wright IJ, Oleksyn J, Machado J-L. **2008**. Scaling of respiration to nitrogen in leaves, stems and roots of higher land plants. *Ecology letters* **11**: 793–801.

Rodríguez-Calcerrada J, Martin-StPaul NK, Lempereur M, Ourcival JM, Rey MC, Joffre R, Rambal S. **2014**. Stem CO_2 efflux and its contribution to ecosystem CO_2 efflux decrease with drought in a Mediterranean forest stand. *Agricultural and Forest Meteorology* **195**–**196**: 61–72.

Rodríguez-Calcerrada J, Salomón RL, Gordaliza GG, Miranda JC, Miranda E, de la Riva EG, Gil L. **2019**. Respiratory costs of producing and maintaining stem biomass in eight co-occurring tree species. *Tree Physiology*.

De Roo L, Bloemen J, Dupon Y, Salomón RL, Steppe K. **2019**. Axial diffusion of respired CO_2 confounds stem respiration estimates during the dormant season. *Annals of Forest Science* **76**: 52.

Rowland L, da Costa ACL, Oliveira AAR, Oliveira RS, Bittencourt PL, Costa PB, Giles AL, Sosa AI, Coughlin I, Godlee JL, *et al.* 2018. Drought stress and tree size determine stem CO_2 efflux in a tropical forest. *New Phytologist* **218**: 1393–1405.

Ryan MG. **1991**. Effects of climate change on plant respiration. *Ecological Monographs* **1**: 157–167.

Salomón RL, Rodríguez-Calcerrada J, Staudt M. **2017**. Carbon losses from respiration and

emission of volatile organic compounds - The overlooked side of tree carbon budgets. In: Gil-Pelegrín E, Peguero-Pina JJ, Sancho-Knapik D, eds. Oaks physiological ecology. Exploring the functional diversity of genus *Quercus* L. Cham: Springer International Publishing, 327–359.

Salomón RL, De Roo L, Bodé S, Boeckx P, Steppe K. **2019a**. Isotope ratio laser spectroscopy to disentangle xylem-transported from locally respired CO_2 in stem CO_2 efflux. *Tree Physiology* **39**: 819-830.

Salomón RL, De Schepper V, Valbuena-Carabaña M, Gil L, Steppe K. **2018**. Daytime depression in temperature-normalised stem CO_2 efflux in young poplar trees is dominated by low turgor pressure rather than by internal transport of respired CO_2. *New Phytologist* **217**: 586–598.

Salomón RL, Steppe K, Crous KY, Noh NJ, Ellsworth DS. **2019b**. Elevated CO_2 does not affect stem CO_2 efflux nor stem respiration in a dry *Eucalyptus* woodland, but it shifts the vertical gradient in xylem [CO_2]. *Plant, Cell & Environment* **42**: 2151–2164.

Salomón RL, Valbuena-Carabaña M, Gil L, McGuire MA, Teskey RO, Aubrey DP, González-Doncel I, Rodríguez-Calcerrada J. **2016**. Temporal and spatial patterns of internal and external stem CO_2 fluxes in a sub-Mediterranean oak. *Tree Physiology* **36**: 1409–1421.

Saveyn A, Steppe K, Lemeur R. **2007**. Daytime depression in tree stem CO_2 efflux rates: Is it caused by low stem turgor pressure? *Annals of Botany* **99**: 477–485.

Saveyn A, Steppe K, Lemeur R. **2008**. Report on non-temperature related variations in CO_2 efflux rates from young tree stems in the dormant season. *Trees* **22**: 165–174.

De Schepper V, Steppe K. **2010**. Development and verification of a water and sugar transport model using measured stem diameter variations. *Journal of Experimental Botany* **61**: 2083–2099.

Sevanto S, McDowell NG, Dickman LT, Pangle R, Pockman WT. **2014**. How do trees die? A test of the hydraulic failure and carbon starvation hypotheses. *Plant, Cell & Environment* **37**: 153–161.

Sorz J, Hietz P. **2006**. Gas diffusion through wood: Implications for oxygen supply. *Trees - Structure and Function* **20**: 34–41.

Steppe K, De Pauw DJW, Lemeur R. **2008**. A step towards new irrigation scheduling strategies using plant-based measurements and mathematical modelling. *Irrigation Science* **26**: 505–517.

Steppe K, De Pauw DJW, Lemeur R, Vanrolleghem A. **2006**. A mathematical model linking tree sap flow dynamics to daily stem diameter fluctuations and radial stem growth. *Tree Physiology* **26**: 257–273.

Steppe K, Saveyn A, McGuire MA, Lemeur R, Teskey RO. **2007**. Resistance to radial CO_2 diffusion contributes to between-tree variation in CO_2 efflux of *Populus deltoides* stems. *Functional Plant Biology* **34**: 785–792.

Steppe K, Sterck F, Deslauriers A. **2015**. Diel growth dynamics in tree stems: linking anatomy and ecophysiology. *Trends in Plant Science* **20**: 335–343.

Sweetlove LJ, Williams TCR, Cheung CYM, Ratcliffe RG. **2013**. Modelling metabolic CO_2 evolution - A fresh perspective on respiration. *Plant, Cell and Environment* **36**: 1631–1640.

Tcherkez G. **2017**. Tracking the orchestration of the tricarboxylic ccid pathway in plants, 80 years after the discovery of the Krebs cycle. In: Tcherkez G, Ghashghaie J, eds. Plant respiration: Metabolic fluxes and carbon balance. Cham: Springer International Publishing, 285–298.

Teskey RO, McGuire MA. **2007**. Measurement of stem respiration of sycamore (*Platanus occidentalis* L.) trees involves internal and external fluxes of CO_2 and possible transport of CO_2 from roots. *Plant, Cell and Environment* **30**: 570–579.

Teskey RO, McGuire MA, Bloemen J, Aubrey DP, Steppe K. **2017**. Respiration and CO_2 fluxes in trees. In: Tcherkez G, Ghashghaie J, eds. Plant Respiration: Metabolic fluxes and carbon balance. Cham: Springer International Publishing, 181–207.

Teskey RO, Saveyn A, Steppe K, McGuire MA. **2008**. Origin, fate and significance of CO_2 in tree stems. *New Phytologist* **177**: 17–32.

Thompson M V., Holbrook NM. **2003**. Application of a single-solute non-steady-state phloem model to the study of long-distance assimilate transport. *Journal of Theoretical Biology* **220**: 419–455.

Tjoelker MG, Oleksyn J, Reich PB. **2001**. Modelling respiration of vegetation: Evidence for a general temperature-dependent Q_{10}. *Global Change Biology* **7**: 223–230.

Trumbore SE, Angert A, Kunert N, Muhr J, Chambers JQ. **2013**. What's the flux? Unraveling how CO_2 fluxes from trees reflect underlying physiological processes. *New Phytologist* **197**: 353–

355.

Wang W, Wang H, Zu Y, Li X, Koike T. **2006**. Characteristics of the temperature coefficient, Q_{10} for the respiration of non-photosynthetic organs and soils of forest ecosystems. *Frontiers of Forestry in China* **1**: 125–135.

Yang J, He Y, Aubrey DP, Zhuang Q, Teskey RO. **2016**. Global patterns and predictors of stem CO_2 efflux in forest ecosystems. *Global Change Biology* **22**: 1433–1444.

Supporting information

Fig. S1 Thickness of the outer tissues (d_{OT}) measured with point dendrometers, and comparison of d_{OT} simulations using linear and non-linear fits.

Fig. S2 Non-linear allometric relationship between stem diameter (D) and thickness of the outer tissues (d_{OT}).

Fig. S3 Temporal variation in xylem CO_2 concentration in the gas phase (xylem [CO_2]) above and below a stem segment monitored in an ancillary maple tree (a), and the resulting vertical gradient (ΔXylem [CO_2]) (b). Corresponding CO_2 concentration dissolved in the sap solution in the liquid phase (sap [CO_2^*]) (c) and the resulting vertical gradient (ΔSap [CO_2^*]) (d)

Table S1 Values of parameters implemented in TReSpire.

Table S2 Sensitivity analysis of submodel C.

Methods S1 Measurements and sensors.

Methods S2 Experiment setup.

Notes S1 Details of TReSpire.

The model (PhytoSim workspace) and the corresponding data that support the findings of this study are openly available in “Mendeley data” at http://dx.doi.org/10.17632/9c9w7mvy9d.2.

Fig 1 Schematic of submodels integrating TReSpire. The "*water flow and storage*" submodel (A) describes the hydraulic functioning of the stem. Driven by sap flow and soil water potential, and calibrated against diameter (D) variations and xylem water potential (Ψ_{XY}), it simulates stem irreversible plastic growth and water content and potential of outer tissues (W_{OT} and Ψ_{OT}). The "*CO_2 sources and fluxes*" submodel (B) is driven by stem temperature and plastic growth, and is calibrated against stem CO_2 efflux. It simulates growth respiration in the cambium (in purple) and maintenance respiration of xylem and outer tissues (in red). Respired CO_2 either radially effluxes to the atmosphere (1-3), dissolves in the sap solution (4) and is transported axially through the xylem (5), or is stored within the stem in gaseous and liquid phases (6). The "*stem carbon balance*" submodel (C) is driven by previous outputs and calibrated against the vertical gradient in stem D variations and the concentration of nonstructural carbohydrates in the stem. It simulates stem carbon sources and sinks (in green and red, respectively): phloem unload (U), sugar-starch interconversion (SSI), stem growth (G), growth and maintenance respiration (R_G and R_M, respectively), and osmoregulatory processes.

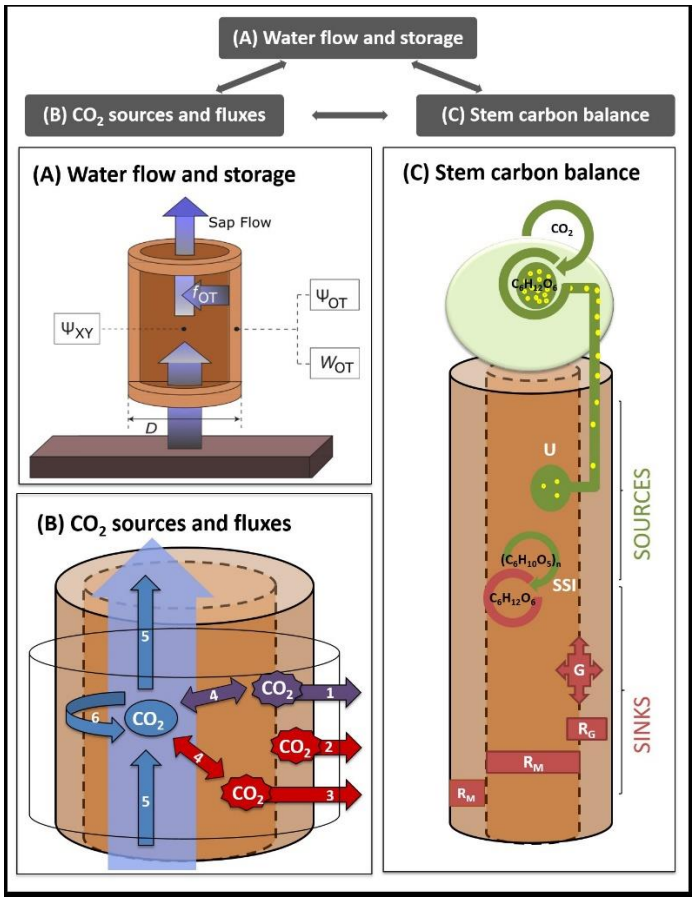

Fig 2 Water flow and storage submodel: (a) Stem diameter measurements (D^{obs}) and simulation (D) with xylem diameter (D_{XY}) and plastic diameter (D_P). (b) Contribution of plastic irreversible growth (ΔD_P), elastic osmotically-driven changes (ΔD_{EO}) and elastic tension-driven changes (D_{ET}) to total stem D fluctuations (ΔD). (c) Measurements of xylem water potential (Ψ_{XY}^{obs}) and simulation of xylem (Ψ_{XY}) and outer tissues (Ψ_{OT}) water potential. The latter results from the sum of osmotic (Ψ_{OT}^{O}) and turgor pressure (Ψ_{OT}^{P}) components. Soil (Ψ_{SOIL}) and root (Ψ_{ROOT}) water potential are also displayed together with the threshold value for irreversible growth (Γ). Shaded areas indicate nighttime.

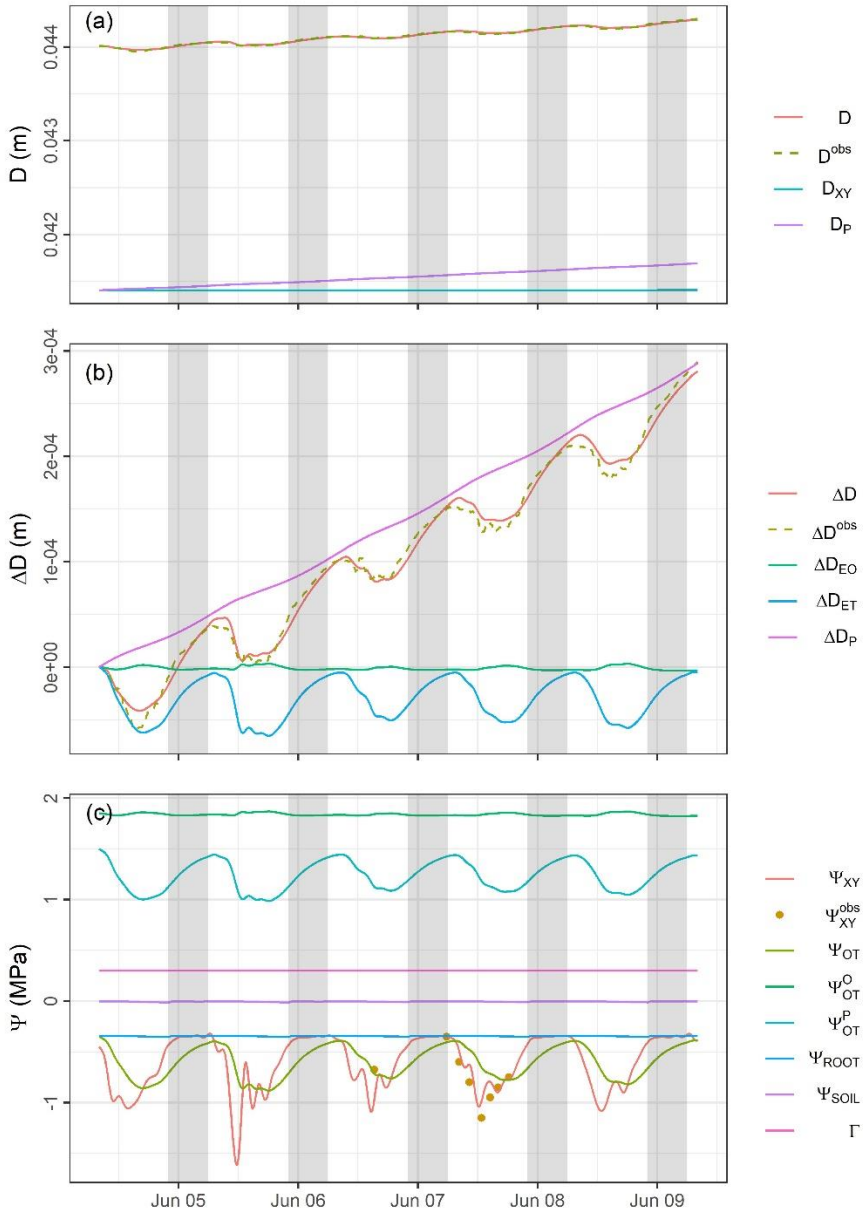

Fig 3 CO_2 sources and fluxes submodel: (a) Partitioning of stem respiration into growth respiration (R_G), maintenance respiration in outer tissues (R_{M_OT}) and maintenance respiration in xylem (R_{M_XY}). (b) Stem respiration (R_S) is the sum of stem CO_2 efflux to the atmosphere (E_A), xylem CO_2 transport through xylem (F_T) and the storage flux, which occurs in the xylem in liquid (ΔS^*_{XY}) and gas (ΔS_{XY}) phases and in outer tissues in the gas phase (ΔS_{OT}). Simulations are calibrated against measurements of E_A (E_A^{obs}). Shaded areas indicate nighttime.

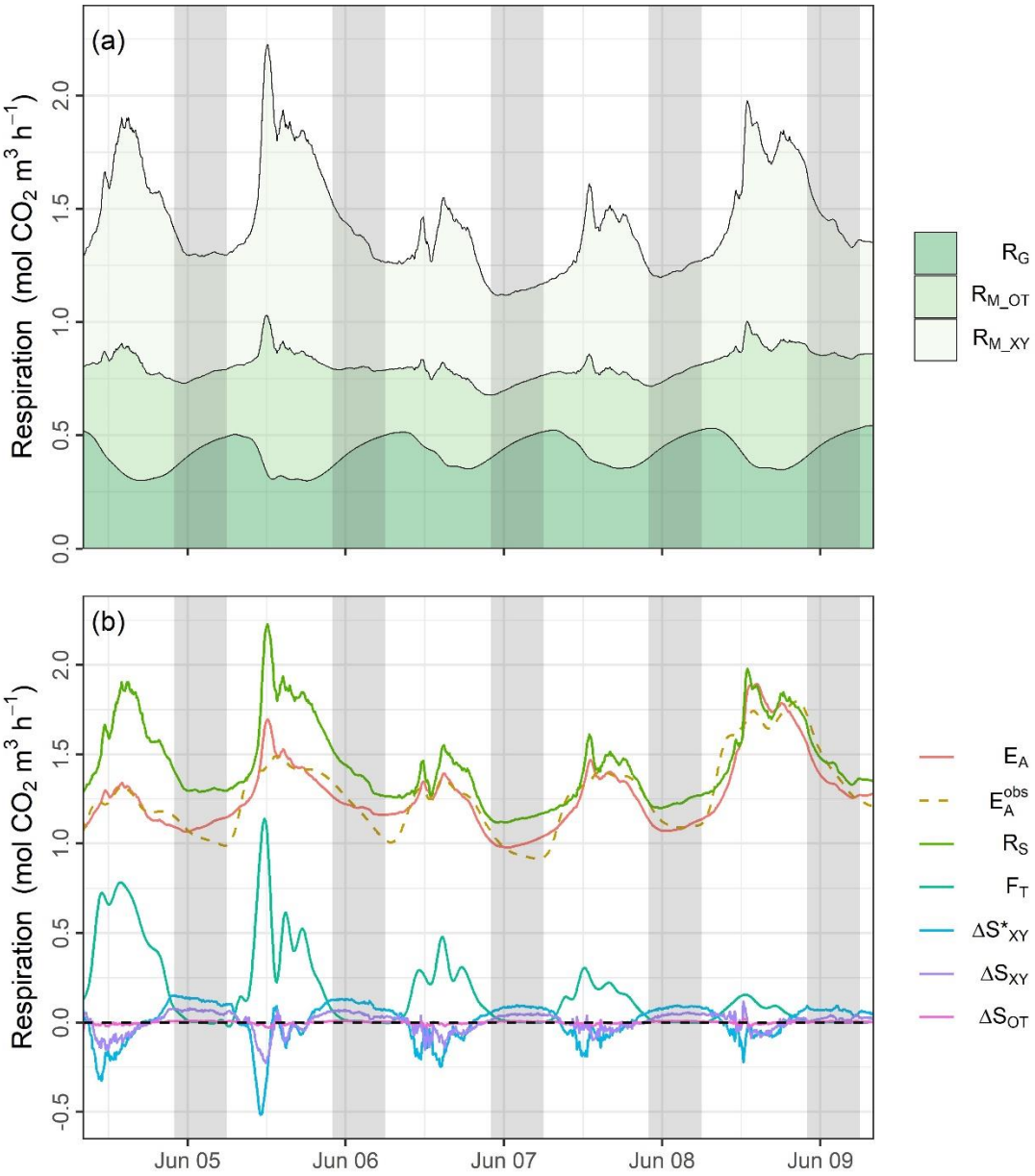

Fig 4 Additional outputs of the CO_2 sources and fluxes submodel (a): Contribution of maintenance respiration of xylem and outer tissues to stem respiration (R_M/R_S), xylem maintenance respiration to stem respiration (R_{M_XY}/R_S), and the ratio of stem CO_2 efflux to stem respiration (E_A/R_S). (b) Concentration of gaseous CO_2 in the xylem ($[CO_2]_{XY}$) and outer tissues ($[CO_2]_{OT}$), and concentration of CO_2 dissolved in the sap solution ($[CO_2^*]$). (c) Sub-daily variation in volume gas fraction (VGF) in the stem and corresponding radial CO_2 diffusivity (Dif). Shaded areas indicate nighttime.

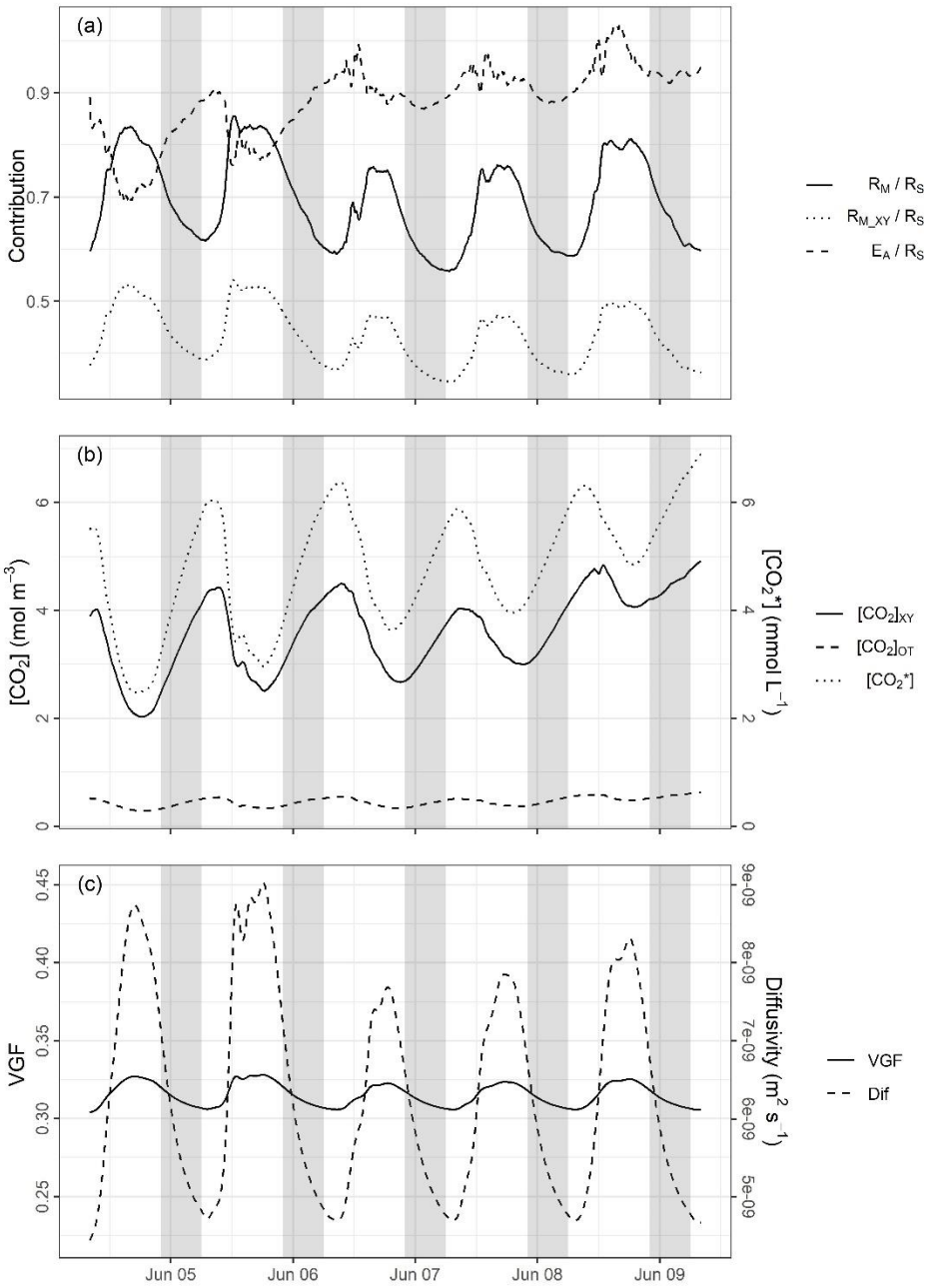

Fig 5 Stem carbon balance submodel: (a) Stem diameter measurements (D_{UP}^{obs}) and simulation (D_{UP}) in the upper part of the stem. (b) Osmotic and pressure components of outer tissues water potential in the upper ($\Psi_{OT\_UP}^{O}$, $\Psi_{OT\_UP}^{P}$) and lower (Ψ_{OT}^{O}, Ψ_{OT}^{P}) part of the stem, and the resulting pressure drop along the stem ($\Delta\Psi_{OT}^{P}$). (c) Concentration of sucrose equivalents ([SU]), starch ([ST]) and target [SU] for starch metabolism ($[SU]_{targ}$). Punctual measurements of [SU] and [ST] used for calibration are shown by the closed circle and square, respectively, whereas [SU] and [ST] simulations are shown by dashed and continuous lines, respectively. (d) Stem carbon sources and sinks: phloem unload (U), stem growth and respiration in sucrose equivalents (G_{SU} and R_{S_SU}, respectively), sugar-starch interconversion (SSI) and osmoregulation (OR). Shaded areas indicate nighttime.

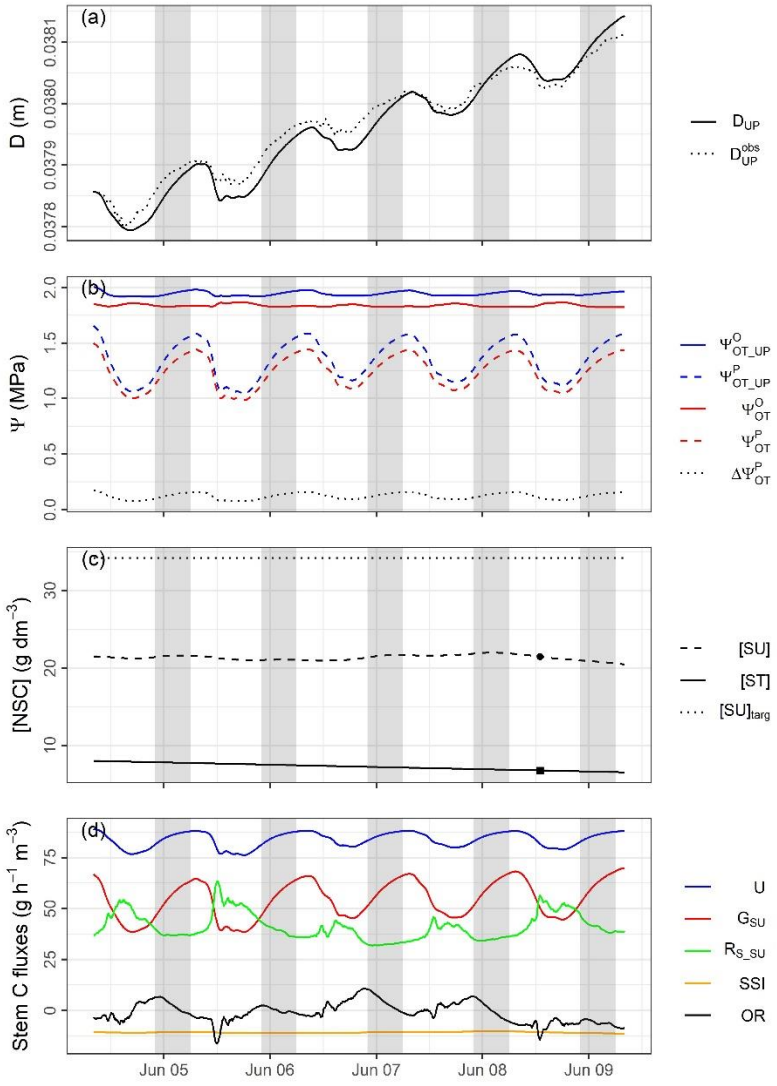

900 **Table 1** Acronym, unit and description of model variables

	Acronym	Unit	Description
Water flow and storage	Ψ_{SOIL}	MPa	Soil water potential
	Ψ_{ROOT}	MPa	Root water potential
	Ψ_{XY}	MPa	Water potential in xylem
	Ψ_{OT}	MPa	Water potential in outer tissues
	Ψ_{OT}^{P}	MPa	Pressure component of Ψ_{OT}
	Ψ_{OT}^{O}	MPa	Osmotic component of Ψ_{OT}
	SF	g h^{-1}	Sap flow through the xylem
	f_{OT}	g h^{-1}	Water exchange between xylem and outer tissues
	F_{SOIL}	g h^{-1}	Root water uptake
	W_{OT}	g	Water content in outer tissues
	V_{OT}	m^3	Volume of the outer tissues
	ε	MPa	Bulk elastic modulus related to elastic changes
	D	m	Stem diameter
	D_{XY}	m	Xylem diameter
	d_{OT}	m	Thickness of the outer tissues
	dD_P/dt	m h^{-1}	Plastic growth changes in D
	dD_{ET}/dt	m h^{-1}	Elastic tension driven changes in D
	dD_{EO}/dt	m h^{-1}	Elastic osmotically driven changes in D
CO_2 sources and fluxes	G	mol C m^{-3} h^{-1}	Stem growth
	R_G	mol CO_2 m^{-3} h^{-1}	Growth respiration
	R_{M_XY}	mol CO_2 m^{-3} h^{-1}	Maintenance respiration in the xylem
	R_{M_OT}	mol CO_2 m^{-3} h^{-1}	Maintenance respiration in outer tissues
	R_S	mol CO_2 m^{-3} h^{-1}	Stem respiration
	T	^oC or ^oK †	Stem temperature
	V_{XY}	m^3	Volume of xylem within the stem segment
	V_S	m^3	Volume of the stem segment
	A_{XY}	m^2	Axial surface of xylem within the stem segment
	A_S	m^2	Axial surface of the stem segment
	k_H	mol atm^{-1} L^{-1}	Henry's law coefficient for CO_2 in water
	k_1		First acidity constant
	k_2		Second acidity constant
	$[CO_2]_{XY}$	mol CO_2 m^{-3}	CO_2 concentration in xylem (gas phase)
	$[CO_2]_{OT}$	mol CO_2 m^{-3}	CO_2 concentration in outer tissues (gas phase)
	$[CO_2^*]$	mol CO_2 L^{-1}	CO_2 concentration dissolved in sap solution
	E_{XY}	mol CO_2 m^{-3} h^{-1}	CO_2 efflux from xylem to outer tissues
	F_T	mol CO_2 m^{-3} h^{-1}	CO_2 transport through xylem
	ΔS_{XY}	mol CO_2 m^{-3} h^{-1}	CO_2 storage flux in the xylem in gaseous phase
	ΔS^*_{XY}	mol CO_2 m^{-3} h^{-1}	CO_2 storage flux in the xylem in liquid phase
	E_A	mol CO_2 m^{-3} h^{-1}	CO_2 efflux from xylem to atmosphere
	ΔS_{OT}	mol CO_2 m^{-3} h^{-1}	CO_2 storage flux in outer tissues in gaseous phase
	Dif	m^2 h^{-1}	Diffusivity

	VGF	$m^3\ m^{-3}$	Volumetric gas fraction
	VWF	$m^3\ m^{-3}$	Volumetric water fraction
	$\Delta[CO_2^*]$	mol $CO_2\ m^{-3}$	Vertical gradient in $[CO_2^*]$
Stem C balance	$\Psi_{OT}{}^{P}{}_{UP}$	MPa	$\Psi_{OT}{}^{P}$ in the upper part of the stem‡
	$\Delta\Psi_{OT}{}^{P}$	MPa	Pressure drop along the stem
	$\Delta[SU]_{OT}$	$g\ m^{-3}$	Drop in [SU] in outer tissues along the stem
	U	$g\ m^{-3}\ h^{-1}$	Phloem unload
	[SU]	$g\ m^{-3}$	Sucrose concentration (in outer tissues)
	[ST]	$g\ m^{-3}$	Starch concentration (in xylem)
	SSI	$g\ m^{-3}\ h^{-1}$	Sugar-starch interconversion
	G_{SU}	$g\ m^{-3}\ h^{-1}$	Growth sink (in sucrose equivalents)
	R_{S_SU}	$g\ m^{-3}\ h^{-1}$	Stem respiration sink (in sucrose equivalents)

Some variables are used in more than one submodel. Classification in this table is made according to their first appearance in the model. † Temperature unit depends on the equation. ‡ Submodel ´water flow and storage´ is partially run for a second time for the upper part of the stem to estimate $\Psi_{OT}{}^{P}{}_{UP}$, in addition to ε_{UP}, V_{OT_UP}, $\Psi_{OT}{}^{P}{}_{UP}$, D_{XY_UP}, d_{OT_UP} and D_{UP}.

Table 2 Acronym, unit and description of model parameters and constants

	Acronym	Unit	Description
Water flow and storage	D_{SOIL}	MPa	Disequilibrium between soil and root Ψ
	R_{XY}	MPa h g^{-1}	Xylem resistance to axial water flow
	R_{OT}	MPa h g^{-1}	Radial resistance to water flow
	C_{OT}	g MPa^{-1}	Capacitance of OT
	ρ_W	g m^{-3}	Water density
	ε_0	m^{-1}	Proportionality constant
	L	m	Stem length
	Γ	MPa	Threshold value for cell growth
	Φ	MPa^{-1} h^{-1}	Extensibility of cell walls related to plastic growth
	k_d	m m^{-1}	Change in OT thickness relative to stem D
	a		Allometric parameter
	b		Allometric parameter
CO_2 sources and fluxes	ρ_{OT}	g m^{-3}	Density of outer tissues
	ρ_{XY}	g m^{-3}	Density of xylem
	C_C	g C g^{-1}	Stem carbon content (on a dry mass basis)
	M_C	g mol^{-1}	Carbon molar mass
	M_N	g mol^{-1}	Nitrogen molar mass
	Y_G	mol C mol C^{-1}	Growth yield
	R_{b_N}	mol CO_2 mol N^{-1} h^{-1}	Basal respiration at a reference T (T_b)
	T_b	°C	Reference temperature
	N_{XY}	g N g^{-1}	Nitrogen concentration in xylem
	N_{OT}	g N g^{-1}	Nitrogen concentration in outer tissues
	Q_{10}		Temperature sensitivity of maintenance R
	pH		Sap pH
	R	m^3 atm K^{-1} mol^{-1}	Ideal gas constant (submodel B)
		m^3 MPa K^{-1} mol^{-1}	Ideal gas constant (submodel C)
	$[CO_2]_{ATM}$	mol CO_2 m^{-3}	Atmospheric CO_2 concentration
	Dif_0	m^2 h^{-1}	Diffusivity at zero VGF
	Dif_e		Exponential parameter of Dif
	$(VWF)_{t0}$	m^3 m^{-3}	Initial volumetric water fraction
	VC_WF	m^3 m^{-3}	Volumetric cell wall fraction
	$(W_{OT})_{t0}$	g	Initial water content in outer tissues
	L_S	m	Length of monitored stem segment
	$\Delta[CO_2^*]_{slope}$	mol CO_2 m^{-3} h^{-1}	Time derivative of $\Delta[CO_2^*]$
C balance	g	MPa m^2 g^{-1}	Gravitational constant
	M_{SU}	g mol^{-1}	Sucrose molar mass
	V_{max}	mol m^{-3} h^{-1}	Michaelis-Menten kinetic parameter
	k_M	mol m^{-3}	Michaelis-Menten kinetic parameter
	k_{starch}	h^{-1}	Kinetic parameter of sugar-starch interconversion
	$[SU]_{targ}$	g m^{-3}	Target sucrose concentration

Some parameters and constants are used in more than one submodel. Classification in this table is made according to their first appearance in the model.

Table 3 Summary of variables needed to run and calibrate the model

Variable	Purpose*	Submodel	Method†
Soil water potential (Ψ_{SOIL})	Input	A	Tensiometer
Sap flow (SF)	Input	A	Heat balance
Stem diameter variations (ΔD)	Calibration	A	LVDT‡
Xylem water potential (Ψ_{XY})	Calibration	A	Pressure chamber
Stem temperature (T)	Input	B	Thermocouple
Stem CO_2 efflux (E_A)	Calibration	B	IRGA
Upper stem ΔD (ΔD_{UP})	Calibration	C	LVDT‡
Soluble sugars concentration ([SU])	Calibration	C	Spectrophotometry
Starch concentration ([ST])	Calibration	C	Spectrophotometry

* Input variables need to be continuously monitored, while calibration variables can be discretely measured. † Method applied in this study case. ‡ Linear Variable Displacement Transducer. An additional LVDT placed at the xylem surface would be necessary if k_d is not derived from measurements in ancillary trees.

Table 4 Parameters and initial values of derivative variables of submodels A and B (mean and 95% confidence interval), and their relative standard error (RSE) and sensitivity indexes against each calibration variable: xylem water potential, stem diameter and stem CO_2 efflux to the atmosphere (Ψ_{XY}, D and E_A, respectively).

Submodel & Parameter		Confidence analysis		Sensitivity analysis		
		Mean [95% CI]	RSE (%)	Ψ_{XY}	D	E_A
A	R_{XY}	1.03×10^{-3} [1.02×10^{-3}, 1.03×10^{-3}]	0.30	198.15	23.98	0.26
	R_{OT}	3.43×10^{-1} [3.35×10^{-1}, 3.51×10^{-1}]	1.17	43.32	3.33	0.13
	C_{OT}	$1.31\times10^{+1}$ [$1.31\times10^{+1}$, $1.32\times10^{+1}$]	0.35	0.94	31.66	0.30
	ε_0	NA		52.33	23.90	0.19
	Φ	9.34×10^{-4} [9.30×10^{-4}, 9.38×10^{-4}]	0.22	32.19	74.19	0.93
B	Y_G	8.18×10^{-1} [8.12×10^{-1}, 8.24×10^{-1}]	0.40	46.81	1.64	4.66
	R_{b_N}	9.95×10^{-3} [9.63×10^{-3}, 1.03×10^{-2}]	1.63	1.47	0.02	1.75
	Q_{10}	$2.18\times10^{+0}$ [$2.10\times10^{+0}$, $2.27\times10^{+0}$]	1.93	4.11	0.14	1.01
	Dif_e	$2.93\times10^{+1}$ [$2.91\times10^{+1}$, $2.94\times10^{+1}$]	0.25	32.52	1.13	7.32
	Dif_0	NA		17.38	0.60	0.82
	$\Delta[CO_2^*]_{slope}$	-5.84×10^{-3} [-5.96×10^{-3}, -5.71×10^{-3}]	1.10	9.11	0.31	0.25
	$(\Delta[CO_2^*])_{t0}$	7.20×10^{-1} [6.96×10^{-1}, 7.44×10^{-1}]	1.68	7.12	0.25	0.50
	$([CO_2^*])_{t0}$	5.50×10^{-3} [5.32×10^{-3}, 5.67×10^{-3}]	1.64	17.70	0.63	0.14
	$([CO_2]_{OT})_{t0}$	5.34×10^{-1} [5.18×10^{-1}, 5.51×10^{-1}]	1.58	10.27	0.35	0.83

NA denote unidentifiable parameters. t0 subscript denote the initial value of derived variables. For calibration and sensitivity analyses, scaling values of measured variables Ψ_{XY}, D and E_A were 0.002 MPa, 3×10^{-6} m and 0.5 mol CO_2 m^{-3} h^{-1}, respectively, according to measurement error standard deviation. Due to the relatively low frequency of Ψ_{XY} measurements, its scaling value was deliberately reduced to increase its objective weight, so that calibration was not biased towards D and E_A. See Table 1 and 2 for the definition of the parameter acronyms.